Published July 13, 2009

The nucleolar RNA methyltransferase Misu (NSun2) is required for mitotic spindle stability

Shobbir Hussain,[1] Sandra Blanco Benavente,[1] Elisabete Nascimento,[1] Ilaria Dragoni,[2] Agata Kurowski,[3] Astrid Gillich,[4] Peter Humphreys,[1] and Michaela Frye[1]

[1]Wellcome Trust Centre for Stem Cell Research, University of Cambridge, Cambridge CB2 1QR, England, UK
[2]Cancer Research Technology Ltd., Cancer Research UK, London WC2A 3NL, England, UK
[3]Goethe University of Frankfurt, Frankfurt am Main 60325, Germany
[4]Wellcome Trust/Cancer Research UK Gurdon Institute, Cambridge CB2 1QN, England, UK

Myc-induced SUN domain–containing protein (Misu or NSun2) is a nucleolar RNA methyltransferase important for c-Myc–induced proliferation in skin, but the mechanisms by which Misu contributes to cell cycle progression are unknown. In this study, we demonstrate that Misu translocates from the nucleoli in interphase to the spindle in mitosis as an RNA–protein complex that includes 18S ribosomal RNA. Functionally, depletion of Misu caused multiple mitotic defects, including formation of unstructured spindles, multipolar spindles, and chromosome missegregation, leading to aneuploidy and cell death. The presence of both RNA and Misu is required for correct spindle assembly, and this process is independent of active translation. Misu might mediate its function at the spindle by recruiting nucleolar and spindle-associated protein (NuSAP), an essential microtubule-stabilizing and bundling protein. We further identify NuSAP as a novel direct target gene of c-Myc. Collectively, our results suggest a novel mechanism by which c-Myc promotes proliferation by stabilizing the mitotic spindle in fast-dividing cells via Misu and NuSAP.

Introduction

The primary function of the nucleolus is the biogenesis of ribosome subunits to ensure efficient translation, but although >700 human proteins stably copurify with nucleoli, only ∼30% of those have functions related to the production of ribosomes (Andersen et al., 2005). Additional nucleolar functions include regulation of specific aspects of mitosis and cell cycle progression (Boisvert et al., 2007). In mitosis, the nucleolus is disassembled, and its components can become redistributed to the cytoplasm or can attach to the surface of condensed chromosomes to support correct chromosome segregation (Gautier et al., 1992; Boisvert et al., 2007; Ma et al., 2007). For the majority of nucleolar proteins, it is unclear whether and how they participate in the regulation of mitosis and cell cycle progression.

The nucleolar protein Misu/NSun2 (Myc-induced SUN domain–containing protein) is a direct downstream target gene of c-Myc in skin required for Myc-induced proliferation and cell cycle progression (Frye and Watt, 2006). In skin, c-Myc induces epidermal stem cells to exit the stem cell compartment, increases proliferation of progenitor cells, and subsequently induces lineage-specific differentiation (Arnold and Watt, 2001; Waikel et al., 2001; Frye et al., 2003; Watt et al., 2008). Misu is expressed at a low level in most tissues, but its expression is increased in a range of tumors. Indeed, inhibition of Misu expression decreases the growth of human squamous cell carcinomas in xenografts (Frye and Watt, 2006), yet the mechanisms by which Misu contributes to c-Myc–mediated cell proliferation remain unknown.

Misu encodes an RNA methyltransferase and defines a new family of mammalian SUN domain–containing genes. The SUN domain was first described in *Escherichia coli* and catalyzes methylation of 16S ribosomal RNA (rRNA; Tscherne et al., 1999). Misu shows highest homology to yeast NCL1 (Trm4), a tRNA methyltransferase, and weak homology to human p120, a protein with substantial homology to the yeast rRNA methyltransferase Nop2 (Wu et al., 1998; King and Redman, 2002;

Correspondence to Michaela Frye: Michaela.Frye@cancer.org.uk

Abbreviations used in this paper: 4-OHT; 4-hydroxytamoxifen; ChIP, chromatin IP; FLICA, fluorochrome inhibitor of caspases; IP, immunoprecipitation; NPM1, nucleolar protein nucleophosmin; NuSAP, nucleolar and spindle-associated protein; QPCR, quantitative real-time PCR; rRNA, ribosomal RNA; Scr RNAi, scrambled RNAi; WCE, whole cell extract.

The Rockefeller University Press $30.00
J. Cell Biol. Vol. 186 No. 1 27–40
www.jcb.org/cgi/doi/10.1083/jcb.200810180

Supplemental Material can be found at:
http://jcb.rupress.org/cgi/content/full/jcb.200810180/DC1

Published July 13, 2009

Brzezicha et al., 2006). During disassembly of the nucleoli in mitosis, Misu is phosphorylated by aurora B kinase, a key regulator of chromosome segregation (Andrews et al., 2003; Sakita-Suto et al., 2007). Phosphorylation of Misu by aurora B suppresses its methyltransferase activity and leads to dissociation from the nucleolar protein nucleophosmin (NPM1; Sakita-Suto et al., 2007). The observation that Misu is phosphorylated by a central mitotic kinase led us to investigate the possibility that Misu might play a role in cell cycle regulation.

In this study, we show that Misu functions not only in nucleoli at interphase but also at mitotic microtubules. Misu and its bound RNA partner are required for proper spindle assembly and chromosome segregation. Misu associates with and regulates the localization of nucleolar and spindle-associated protein (NuSAP), an essential spindle assembly factor.

Results

Misu is nucleolar in interphase and interacts with mitotic microtubules

To determine the exact cellular localization of Misu throughout the cell cycle, we labeled HCC1954 cells using antibodies targeting Misu and α-tubulin. HCC1954 is a breast cancer cell line with a fivefold increase in Misu expression when compared with normal breast tissue (unpublished data) and was used to analyze the function of Misu throughout this study. As expected, Misu colocalized with NPM1 in nucleoli of interphase cells (Fig. 1 A, arrows) and decorated the mitotic spindle during cell division in HCC1954 cells (Fig. 1 A, arrowheads; Frye and Watt, 2006; Sakita-Suto et al., 2007).

Localization of Misu varied with the cell cycle. In prophase of the cell cycle, Misu was not associated with microtubules (Fig. 1 B, arrows) but localized to the pericentriolar material (Fig. 1 B, arrowheads). In metaphase and anaphase, Misu staining overlapped with the spindle (Fig. 1, C and D, arrows). In telophase, Misu was localized to the midbody (Fig. 1 E, arrows). We confirmed that Misu was associated with soluble tubulin by reciprocal coimmunoprecipitations (co-IPs; Fig. 2, A and B). Given that tubulin is a very abundant protein, we tested whether the association of Misu and tubulin was cell cycle dependent. Indeed, Misu and tubulin coprecipitated in M but not G1 phase of the cell cycle (Fig. 2 C, G1 and M). To test the specificity of the Misu antibody, we performed co-IPs in cells expressing an RNAi construct for Misu and found no association of Misu and tubulin (Fig. 2 C, scrambled RNAi [Scr RNAi] and Misu RNAi). We conclude that Misu only became fully associated with the spindle in metaphase but remained associated with microtubules through to cytokinesis.

To confirm that our antibody specifically detected Misu at the spindle, we overexpressed the full-length protein in T47D cells, a breast cancer cell line with low endogenous Misu expression (Fig. S1, A and B; and unpublished data). Ectopically expressed Misu (pBabe-Misu) preferentially stained at the spindle relative to empty vector controls (pBabe; Fig. S1, A and B). We further confirmed the localization of Misu at the spindle by repeating these experiments using a second polyclonal antibody raised against a distinct peptide region of the Misu protein (EF2; Fig. S1, C and D). The results were identical and consistently showed that Misu is a spindle-associated protein.

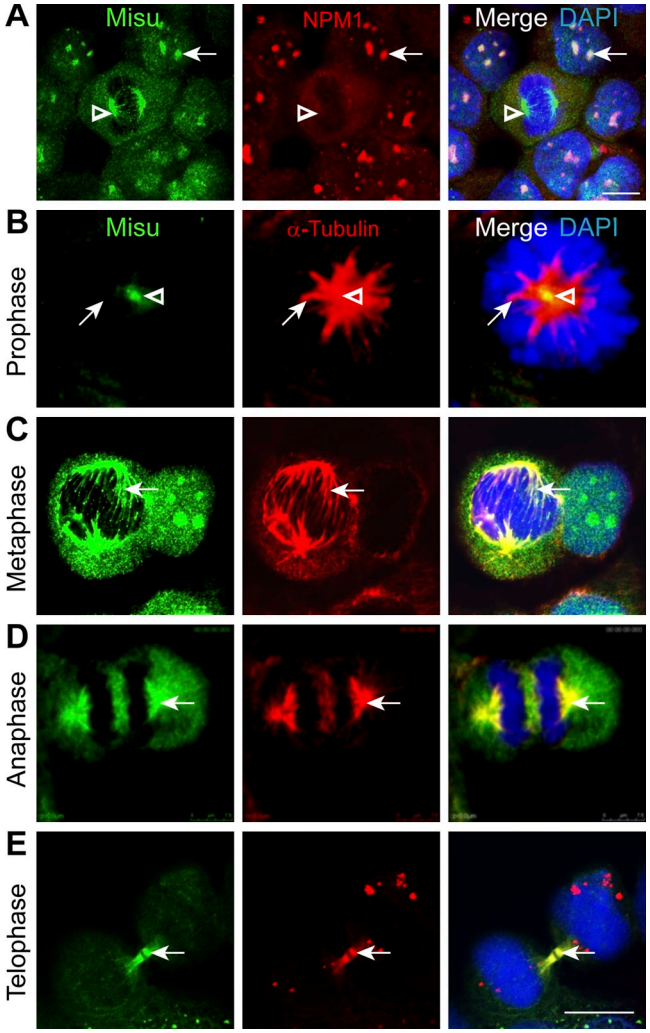

Figure 1. **Misu is nucleolar in interphase and associates with tubulin at the spindle in mitosis.** (A) Misu (green) colocalizes with NPM1 (red) at the nucleolus (arrows) but not at the spindle (arrowheads). (B) In prophase, Misu was found at pericentriolar material (arrowheads) but not the spindle fibers (α-tubulin; arrows). (C and D) In metaphase and anaphase, Misu colocalizes with α-tubulin along the spindle (arrows). (E) In telophase, Misu and α-tubulin localize to the midbody (arrows). DNA is counterstained with DAPI (blue). Bars, 10 μm.

Expression of Misu is required for correct spindle assembly

To determine the function of Misu at mitotic microtubules, we inhibited the expression of Misu by retroviral infection of an RNAi construct into HCC1954 (Frye and Watt, 2006). When compared with an Scr RNAi construct, virtually all cells (>99%) transduced with Misu RNAi expressed undetectable levels of Misu (Fig. S2, A–D). In response to inhibition of Misu, only ∼20% of all cells underwent normal mitosis (Fig. 3, A–D and F [normal mitosis]).

The most striking observation after Misu depletion was the formation of unstructured spindle fibers that coincided with misaligned chromosomes failing to congress properly at the metaphase plate (Fig. 3 B). In >60% of mitotic cells, spindle fibers

Published July 13, 2009

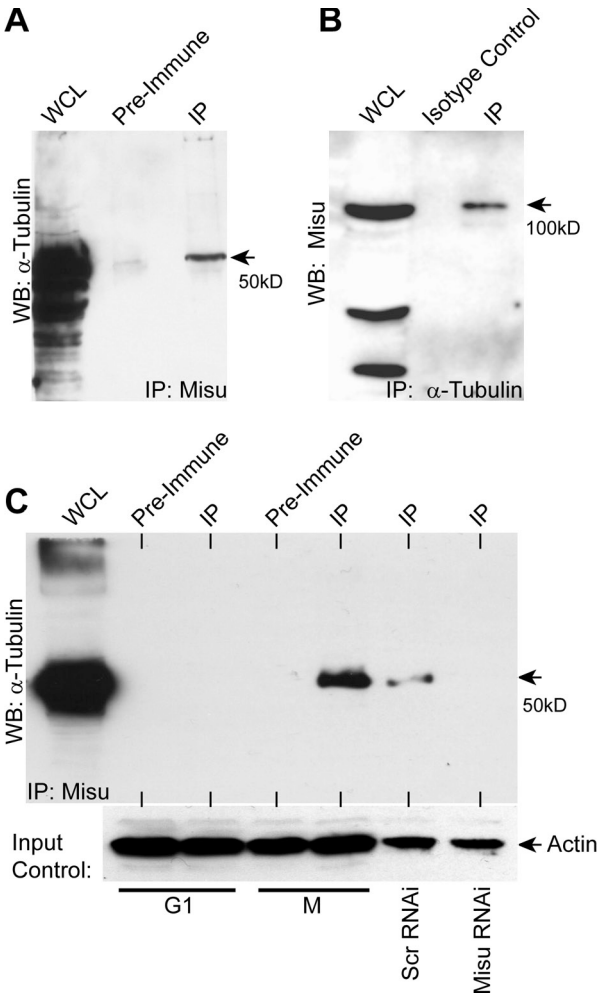

Figure 2. **Misu coimmunoprecipitates with α-tubulin only in mitosis.** (A and B) Misu reciprocally coimmunoprecipitates with α-tubulin in HCC1954 cells. (C) Misu only associates with α-tubulin in M phase of the cell cycle. No interaction can be detected when Misu is depleted by RNAi (Misu RNAi). Actin was used a loading control. WCL, whole cell lysate; WB, Western blot. The arrow indicates the size of the proteins.

lacked their normal smooth structure and appeared irregular in orientation with the main body of associated chromosomes extending even beyond the spindle poles (Fig. 3, B [arrows] and F [abnormal spindle structure]). Individual chromosomes were often misaligned (Fig. 3 C, arrows), and the number of mitotic cells with multipolar spindles increased approximately threefold when compared with controls (Fig. 3, C [arrowheads] and F). Finally, the distribution of chromosomes between multipolar spindles appeared nonuniform, and in anaphase of the cell cycle, individual chromosomes were pulled away from either one or both of the main bodies of chromosomes (Fig. 3 D, arrows).

We tested whether the loss of spindle integrity and the formation of multipolar spindles lead to impaired chromosome segregation in anaphase. Indeed, only 40% of cells in interphase were mononuclear, and the number of polynucleated cells increased dramatically (Fig. 3, E and G). Almost 50% of all cells were polynucleated, and these cells often contained ≥1 micronuclei (Fig. 3, E and G). Micronuclei were typically within the size range of 20–120 μm^2, and unbiased computational measurements indicated that the frequency of micronuclei increased around sixfold in response to Misu RNAi (36.1%) compared with control cells (5.7%; Fig. 3 H, Scr RNAi). This observation was consistent with the increase of mitotic cells with multipolar spindles.

To confirm the specificity of the spindle phenotype in response to depletion of Misu, we reproduced the RNA experiment with an siRNA duplex with distinct sequence from the RNAi construct described in Fig. 3 (Fig. S2, D and E). To further demonstrate that the effect on the spindle was direct, control and Misu siRNA–transfected HCC1954 cells were synchronized in M phase of the cell cycle using nocodazole block. After a 45-min recovery period from nocodazole block, the spindle morphology was assessed in the first mitosis after knockdown of Misu (Fig. 4). Depletion of Misu using the siRNA duplex in synchronized HCC1954 cells caused mitotic defects similar to those seen in unsynchronized cells, including abnormal spindle structure, misaligned mitotic chromosomes (Fig. 4, A–C, arrows), and multipolar spindles (Fig. 4, A–C [arrowheads] and D [HCC1954]). When cells were arrested in mitosis using nocodazole, control siRNAi and Misu siRNAi cells accumulated in M phase to a similar extent, suggesting that cells depleted of Misu are unable to overcome nocodazole block and that Misu is therefore unlikely to be involved in spindle checkpoints (Fig. 4 E).

To test whether other cell lines show the same mitotic defects in response to depletion of Misu, we infected four more breast cancer cell lines with Misu RNAi (Fig. S2, G–N). BT20 and MT3 express high levels and Cal51 and PMC42 express lower levels of Misu on protein and RNA level (Fig. S2, G–J, top; and not depicted), yet all cell lines showed similar mitotic defects (Fig. S2, G–N). In all cell lines, Misu localized to both the nucleoli and the spindle (Fig. 4, F and G; and not depicted). Synchronized Cal51 cells had mitotic defects comparable with HCC1954 cells (Fig. 4, A–D and H). We conclude that inhibition of Misu leads directly to impaired spindle assembly in numerous cancer cell lines independent of relative levels of endogenous Misu expression.

We considered the possibility that the formation of micronuclei in response to Misu RNAi was an indirect effect caused by DNA double-strand breaks. DNA damage can be visualized by increased phosphorylation of histone γH2A.X (Rogakou et al., 1998). However, Misu RNAi cells did not exhibit higher levels of phosphorylated histone γH2A.X compared with controls (Fig. S3, A–C). Collectively, our results observed that mitotic defects in Fig. 3 appear to be a direct consequence of loss of Misu.

Depletion of Misu induces cellular apoptosis

Knockdown of Misu had multiple adverse effects on spindle integrity, finally resulting in increased aneuploidy, which in cancer cells often leads to a higher frequency of apoptosis. To test whether aneuploid HCC1954 cells undergo apoptosis in response to inhibition of Misu, we measured caspase activity using flow cytometry (Fig. 5, A and B). We found that the percentage of cells undergoing cell death increased in cells transduced with Misu RNAi (11.3%) relative to cells infected with an Scr RNAi construct (0.6%; Fig. 5, A and B). Cells treated with actinomycin D were used as a positive control for apoptosis (34.5%; Fig. 5, A and B). The percentage of necrotic cells in response to Misu

Published July 13, 2009

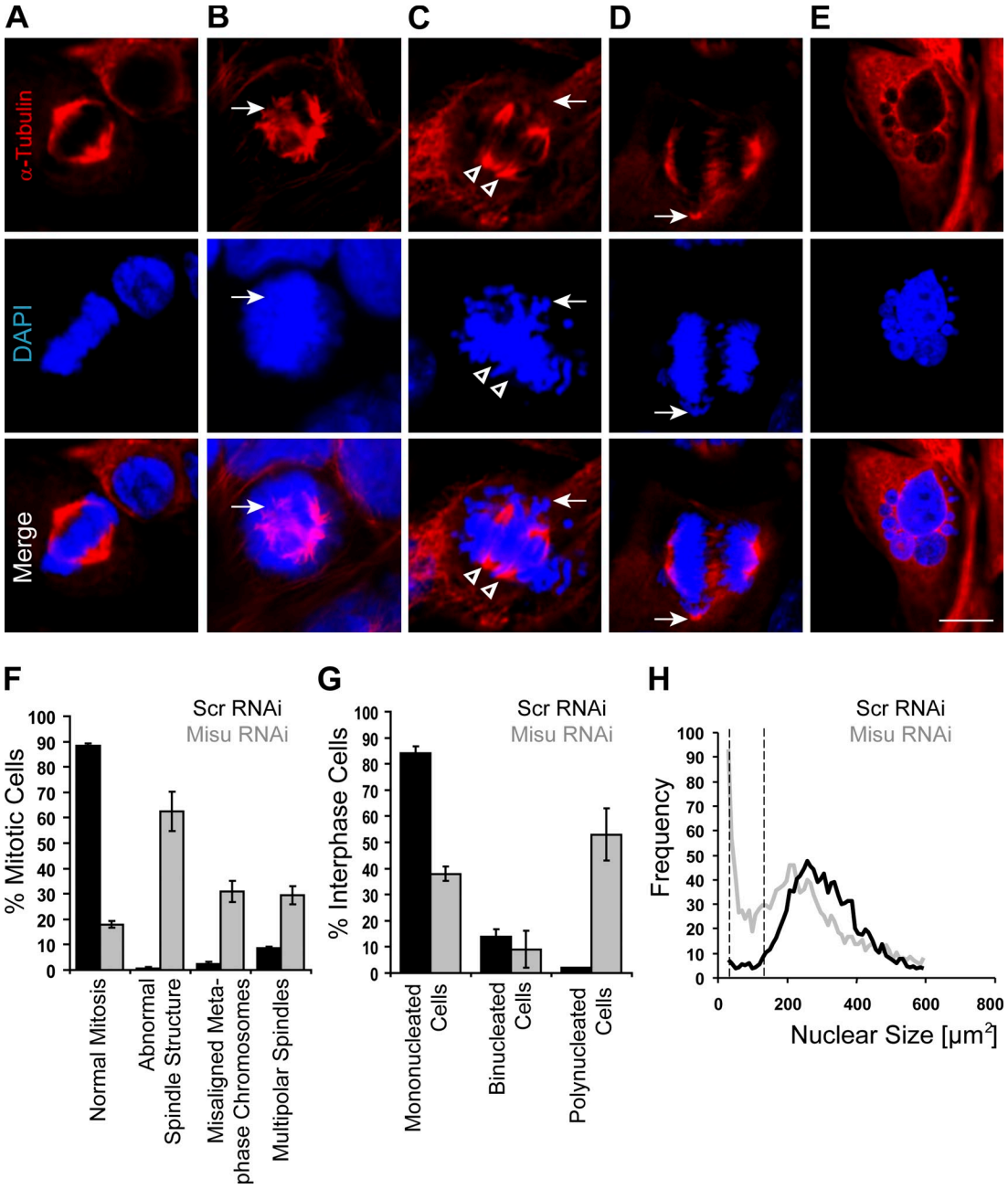

Figure 3. **Depletion of Misu in HCC1954 cells results in impaired spindle formation.** (A) Cells infected with an Scr RNAi display normal mitosis. (B–D) Misu RNAi results in several adverse effects on mitosis. Chromosomes extend beyond the spindle poles (B, arrows), multipolar spindles (C, arrowheads), individual chromosomes that are misaligned (arrows), and those that are pulled away from the main body of chromosomes (D, arrows) in anaphase. (E) Number of micronuclei in interphase cells increased. Cells are stained for α-tubulin (red) and DAPI (blue). Bar, 10 μm. (F and G) Quantification of effects of Misu RNAi in mitotic cells (F) and interphase cells (G) compared with Scr RNAi. (H) Automated quantification of number of micronuclei in Misu RNAi and Scr RNAi cells. Dotted lines indicate the typical size range of micronuclei. Error bars indicate mean ± SD.

RNAi (8.1%) was comparable with control cells (7.4%; Scr RNAi), confirming that cell death was caused by apoptosis (Fig. 5 C). Thus, the expression of Misu in HCC1954 cells prevents apoptosis.

Misu specifically binds 18S rRNA at the spindle

The unexpected finding that an RNA methyltransferase may be associated with mitotic spindle function is not entirely unprecedented; recently, another RNA–protein complex containing the mRNA export factor Rae1 has been found to localize to the spindle (Blower et al., 2005). Strikingly, RNA molecules themselves were found to be directly required for spindle assembly in *Xenopus laevis* egg extracts (Blower et al., 2005). We therefore considered the possibility that Misu and its RNA-binding partner may play a role in spindle assembly.

Like other RNA methyltransferases, Misu methylates a range of RNAs, including tRNAs and rRNAs in vitro, but its substrates in vivo are not well defined (Obara et al., 1982; Frye

Published July 13, 2009

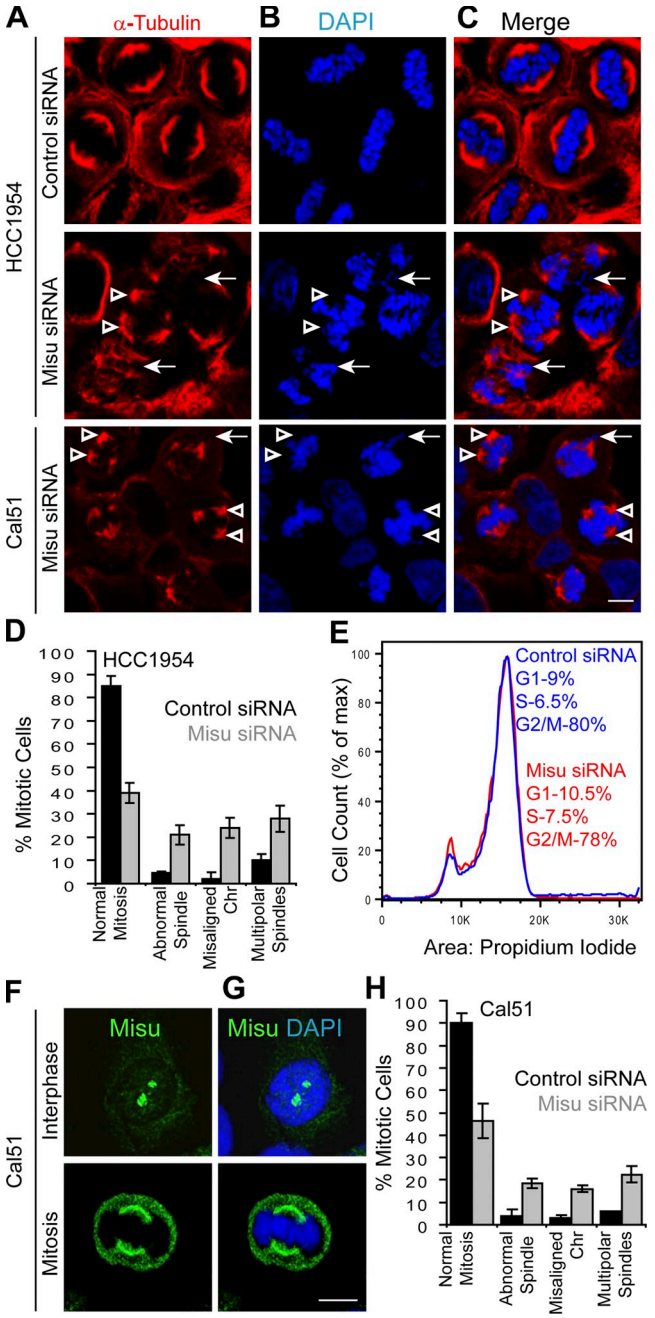

Figure 4. **Depletion of Misu directly induces mitotic defects.** (A–C) Synchronized HCC1954 and Cal51 cells transfected with control and Misu siRNA in the first cell cycle after depletion of Misu. Cells were analyzed after a 45-min recovery period after nocodazole arrest. Depletion of Misu by siRNA (Misu siRNA) causes formation of multipolar spindles (arrowheads) and misaligned chromosomes (arrows). Cells are stained for α-tubulin (A, red) and DAPI (B, blue). (D) Quantification of effects of Misu siRNA in mitotic HCC1954 cells. (E) Control and Misu siRNA cells accumulate to a similar extent in M phase after nocodazole block. (F and G) In Cal51 cells, Misu (green) localizes to nucleoli in interphase and the spindle in mitosis. DNA is counterstained with DAPI. (H) Quantification of effects of Misu siRNA in mitotic Cal51 cells. Chr, Chromosomes. Error bars indicate mean ± SD. Bars, 10 μm.

and Watt, 2006). To identify endogenous RNA-binding partners of Misu, we performed IPs for endogenous Misu in HCC1954 cells and isolated Misu-bound RNA from the resulting lysate (Fig. 6 A, left). A target RNA species with the size of 1.9 kb was specifically enriched relative to preimmune serum (Fig. 6 A, left, asterisks). Treatment of the lysate with RNaseA confirmed that RNA was immunoprecipitated (Fig. 6 A, right, asterisks).

We reasoned that a strong, distinct RNA band could be a component of the ribosome, as ribosomal-associated noncoding RNAs are among the most prevalent in cells. Eukaryotic ribosomes contain four different rRNA molecules: 18S, 5.8S, 28S, and 5S. The RNA band we observed was a single band of ∼1.9 kb, potentially corresponding to 18S rRNA. To confirm that the RNA species was indeed 18S rRNA, we reverse transcribed the purified RNA and performed a PCR using 18S rRNA–specific primers (Fig. 6 B, top). Although no other rRNA species was detectable by co-IP with Misu (Fig. 6 A), we considered the possibility that small rRNAs such as 5S and 5.8S might be present in the samples. Their small sizes make them difficult to visualize on agarose gels stained with ethidium bromide, and we did observe a low molecular mass nonspecific band at ∼0.5 kb (Fig. 6 A), which may have obscured the presence of small rRNAs. However, RT-PCR analysis revealed that neither 5S nor 5.8S rRNA coimmunoprecipitated with Misu (Fig. 6 B, bottom). These results suggested that Misu bound exclusively 18S rRNA.

To test whether the interaction between Misu and 18S rRNA is dependent on translation, we treated the cells with puromycin, a compound that causes premature chain termination during translation, and performed IPs for endogenous Misu (Fig. 6 C). We isolated comparable levels of Misu-bound RNA in untreated and puromycin-treated cells (IP) and again confirmed by RT-PCR that we precipitated 18S rRNA in both cases (Fig. 6 C). To investigate the cell cycle dependency of Misu–RNA binding, we synchronized the cells in G1 and M phases of the cell cycle (Fig. 6 D). We immunoprecipitated similar levels of 18S rRNA in synchronized and unsynchronized cells (IP) and confirmed by RT-PCR that we precipitated 18S rRNA (Fig. 6 D). Our data demonstrated that Misu associates with 18S rRNA not only in interphase but also during mitosis.

To determine the extent of colocalization of Misu and 18S rRNA in HCC1954, we designed an Alexa Fluor 488–labeled DNA probe directed against 18S rRNA. As expected, the 18S rRNA probe strongly stained the nucleoli where synthesis and methylation of rRNA take place (Fig. 6 E, asterisk; Liau and Hurlbert, 1975). We also observed 18S rRNA along the mitotic spindle (Fig. 6 E, left, arrow). 18S rRNA did not appear to localize to the entire length of mitotic spindle fibers but was consistently enriched toward the spindle poles. To confirm that we indeed detected RNA, we treated the cells with RNaseA, which resulted in loss of staining at both the spindle and nucleoli (Fig. 6 E, +RNaseA; and not depicted). We further confirmed the specificity of the 18S rRNA probe by incubating the antisense probe with the corresponding sense oligo before staining and observed a complete loss of staining at both the nucleoli and spindle (Fig. S3, D and E). Costaining for Misu and 18S rRNA confirmed an identical cellular distribution at nucleoli and the spindle (Fig. S3 F).

Localization of Misu at the spindle and spindle stability is dependent on RNA

We next asked whether RNA is required for the localization of Misu to the spindle. We treated cells with RNaseA or PBS (control) for 15 min before fixation and immunofluorescence analysis.

Published July 13, 2009

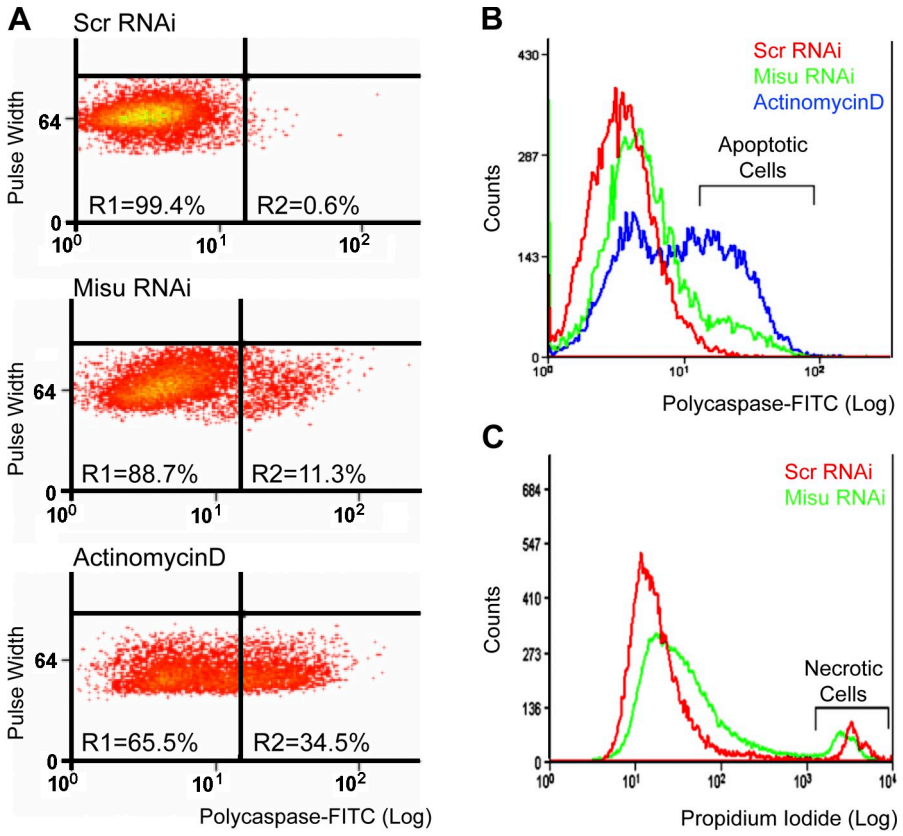

Figure 5. **Apoptosis but not necrosis is increased in response to Misu depletion.** (A) Flow cytometry to measure cell death and apoptosis using FLICA polycaspase probes in HCC1954 cells infected with Scr RNAi (top), Misu RNAi (middle), and cells treated with actinomycin D as control (bottom). (B and C) Apoptosis is increased in cells with Misu RNAi (B), but necrosis is unchanged (C), as measured by staining with propidium iodide before FACS analysis.

When treated with RNaseA, Misu was lost from the spindle fibers but not the spindle poles (Fig. 6 G, arrows) in the vast majority of mitotic cells (Fig. 6, F–H). The loss of Misu exclusively at the spindle fibers demonstrated that the treatment had not resulted in indiscriminate depletion of proteins at microtubules and that RNA is required for the localization of Misu to the spindle.

In response to RNaseA treatment, the morphology of the mitotic spindle was greatly disturbed (Fig. 6 G; and Fig. 7, A and B, α-tubulin). These spindle abnormalities were similar to those observed when Misu expression was repressed by RNAi (Fig. 3 and Fig. 7 C). Chromosomes showed a diffuse arrangement at the metaphase plate and extended beyond the spindle poles (Fig. 7, A–C, arrowhead). In some cases, individual chromosomes were misaligned (Fig. 7, A–C, arrows). Our data suggest that both Misu and RNA are required for spindle stability. However, spindle localization of 18S rRNA was independent of Misu because 18S rRNA localized to spindles even in the absence of Misu (Fig. S4, A–C).

Misu regulates spindle stability independent of translation and its methyltransferase activity

The role of posttranscriptional modifications on RNA, including methylation, is to ensure translation fidelity (Agris, 2004; Grosjean, 2005). Thus, the formation of a complex containing Misu and 18S rRNA at mitotic microtubules led us to speculate that Misu is involved in active protein synthesis at the spindle (Eliscovich et al., 2008). To test whether the localization of 18S rRNA is dependent on active translation, we treated the cells with puromycin. The localization of neither 18S rRNA nor Misu was affected by puromycin, confirming that active translation was not required to localize 18S rRNA or Misu to the spindle (Fig. 7, D–F; and Fig. S4, D and E).

To analyze whether the methyltransferase activity of Misu is required for the mitotic phenotype, we asked whether enzymatic dead mutants of Misu rescue spindle defects caused by Misu depletion. We generated enzymatic dead mutants of Misu by introducing point mutations (Fig. 8 A). In three mutant constructs, we replaced aspartic acid 268, cysteine 271, and cysteine 321 with alanine (D268A, C271A, and C321A). In a fourth construct, the lysine at position 190 was substituted with methionine (K190M). Those residues have been extensively characterized in yeast to be essential for RNA target substrate binding (D268A, C271A, and C321A) or ligand binding (K190M; S-adenosyl-L-methionine) and are conserved through eukaryotic evolution (King and Redman, 2002; Bujnicki et al., 2004).

Equal amounts of purified proteins were used to test their methyltransferase activity in vitro (Fig. 8, A and B). The point mutation C271A generated a protein that irreversibly bound RNA substrates and thus ran at higher molecular weight (Fig. 8 A, asterisk; King and Redman, 2002). Fig. 8 B demonstrated that none of the mutant constructs can methylate RNA substrates such as tRNA in vitro. We next generated constructs for wild-type Misu and two of the mutants (K190M and D268A) that were resistant to Misu RNAi by introducing silent mutations into the RNAi target site. These constructs were then coinfected with Misu RNAi or a control RNAi (Scr RNAi) into HCC1954 cells (Fig. 8 C). Western blot analysis revealed that cells infected

Published July 13, 2009

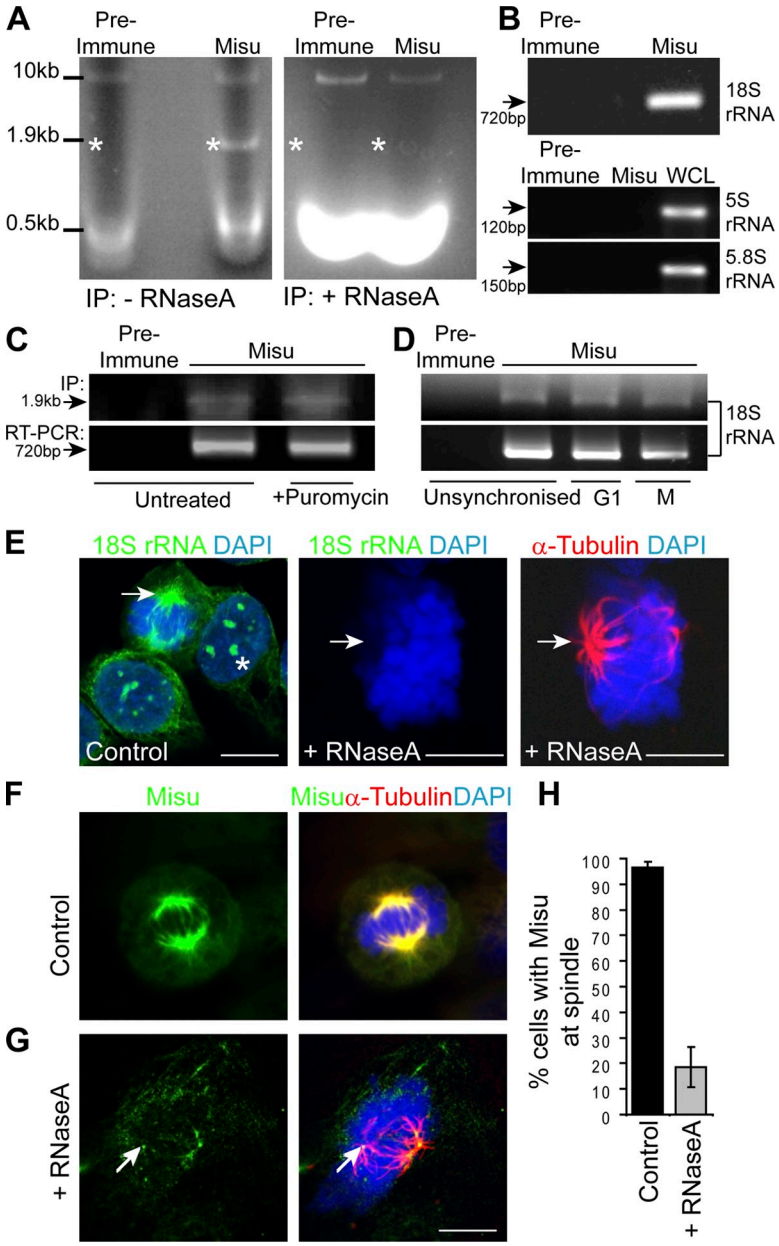

Figure 6. **Identification of 18S rRNA as binding partner of Misu at nucleoli and the spindle.** (A) IP using a Misu antibody or preimmune serum followed by an RNA isolation. RNA with the size of 1.9 kb binds to Misu (left, asterisks) and is degraded in response to RNaseA (right, asterisks). (B) Gene-specific PCR of reverse-transcribed purified RNA identifies 18S rRNA (top) but not 5S or 5.8S rRNA (bottom) as binding partner of Misu. (C and D) IP and RT-PCR in untreated and puromycin-treated cells (C) and unsynchronized versus cells synchronized in G1 and M phase of the cell cycle (D). (E, left) Localization of 18S rRNA (green) using an Alexa Fluor 488–conjugated DNA probe at the nucleoli (asterisk) and the spindle (arrows). (middle and right) Treatment with RNaseA depletes 18S rRNA from the spindle (+RNase). (F and G) Treatment with RNaseA depletes Misu from the spindle but not the spindle poles (arrow). Cells are stained with Misu (green), α-tubulin (red), and DAPI (blue). (H) Quantification of RNase effect on localization of Misu to the spindle. Error bars indicate mean ± SD. Bars, 10 μm.

with RNAi-resistant wild-type Misu (pB-Misu-R) or resistant Misu mutants (pB-K190M-R and pB-D268A-R) were indeed insensitive to Misu RNAi and expressed similar levels of Misu as control cells (pB-Empty + Scr RNAi; Fig. 8 C).

When analyzed for mitotic defects, we found that co-expression of Misu-R and Misu RNAi corrected the spindle phenotype back to levels found in control cells (pB-Empty + Scr RNAi; Fig. 8, D and E). Importantly, we also found that the catalytically inactive mutants K190M-R and D268A-R rescued the Misu–RNAi spindle phenotype to a similar extent (Fig. 8, D and E). These results show that the methyltransferase activity of Misu is dispensable in its role in regulating spindle stability.

Misu recruits NuSAP to the spindle

We sought to identify spindle assembly factors through which Misu regulates spindle stability. The small GTPase Ran mediates spindle assembly through the importin-α and -β dimer, which binds to nuclear localization sequences of spindle assembly factors (Clarke and Zhang, 2008). Misu protein has a putative nuclear localization sequence (KKDGVCGPPPSKKMK), suggesting that Misu could be either a direct target of the importin-α and -β dimer or an indirect target via interactions with other spindle assembly factors. To test this hypothesis, we analyzed whether Misu interacts with known direct mitotic targets of RanGTP in spindle assembly (TPX2, NuMA, and NuSAP) or indirect targets with vital roles in mitotic spindle assembly (TACC [transforming acidic coiled coil] and aurora A; Gruss et al., 2001; Nachury et al., 2001; Wiese et al., 2001; Trieselmann et al., 2003; Tsai et al., 2003; Albee et al., 2006; Ribbeck et al., 2006; Sato and Toda, 2007).

We analyzed whether the localization of spindle assembly factors is dependent on the presence of Misu. Out of all factors analyzed, only the localization of NuSAP was affected when Misu was depleted by RNAi (Fig. 9, A–C; and Fig. S5, A–G).

Published July 13, 2009

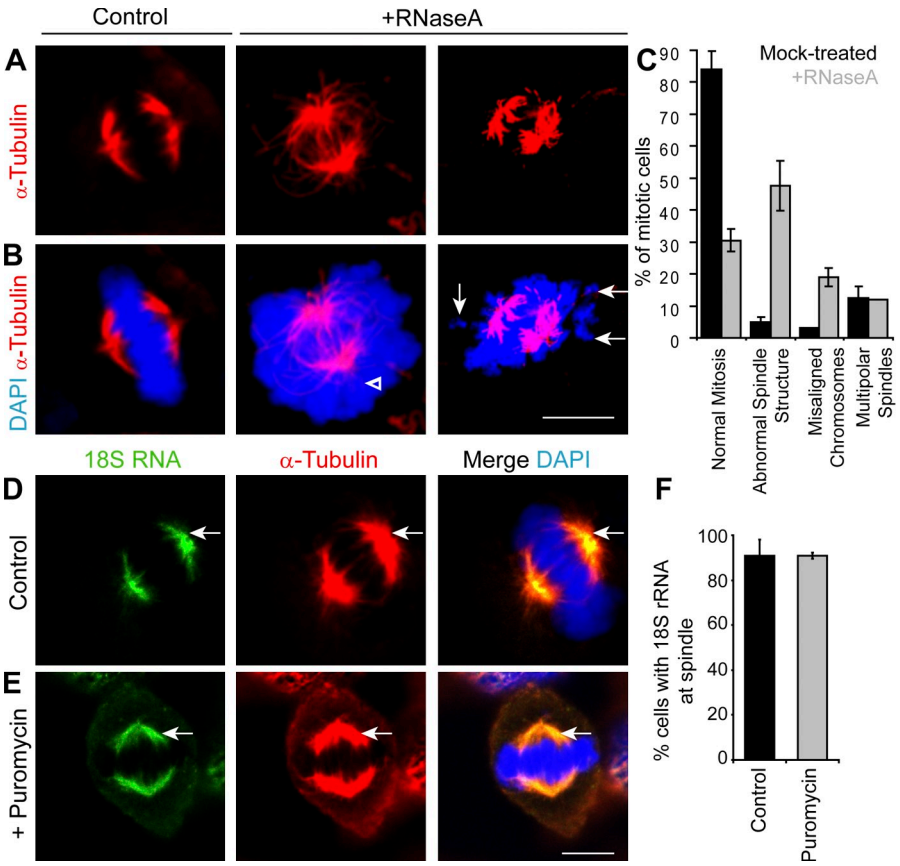

Figure 7. **Treatment with RNaseA disrupts spindle morphology, and localization of 18S rRNA to the spindle is independent of active translation.** (A–C) Spindle shows diffuse arrangement when cells were treated with RNaseA compared with control. Chromosomes extend beyond the spindle poles (arrowhead), and individual chromosomes are misaligned (arrows). (D–F) Localization of 18S rRNA (green) at the spindles (arrows) is not affected by treatment with puromycin compared with cells treated with PBS (control). Cells are counterstained with α-tubulin (red) and DAPI (blue). Error bars indicate mean ± SD. Bars, 10 μm.

Upon Misu removal, NuSAP failed to localize to the mitotic spindle in metaphase (Fig. 9, A–C [arrowheads] and G), but the localization of NuSAP to the spindle poles was unchanged (Fig. 9, A–C, arrows). The nucleolar localization of NuSAP in interphase was also not affected by depletion of Misu (Fig. 9, D–F [arrows] and H).

We found that NuSAP colocalized with Misu at the mitotic spindle distal to chromosomes and spindle poles in metaphase of HCC1954 cells (Fig. 9, A–C). Although the localization of NuSAP to the distal spindle has been observed by others (Raemaekers et al., 2003), the staining at the spindle poles is considered to be nonspecific because GFP-tagged NuSAP does not localize to the spindle poles (unpublished data; G. Carmeliet, personal communication). This observation is consistent with our finding that the NuSAP antibody still stains the spindle poles in Misu-depleted cells (Fig. 9 A, Misu RNAi).

However, in mouse MC3T3E1 osteoblasts, NuSAP localizes mainly to the central spindle and adjacent to chromosomes in metaphase and early anaphase (Raemaekers et al., 2003). Occasionally, we observed NuSAP at both the spindle distal and adjacent to chromosomes in HCC1954 cells, but in the vast majority of cells, NuSAP stained the distal spindle with higher intensity (Fig. S4, F and H). In anaphase, when cells were fixed in methanol, NuSAP labeled both the central and distal spindle (Fig. S4 G). However, NuSAP labeled only the central spindle when cells were fixed with paraformaldehyde (Fig. S4 I; Raemaekers et al., 2003). Because we used the same antibodies as prior experiments for NuSAP, we conclude that this discrepancy in NuSAP localization was caused by cell type–specific localization of NuSAP at the spindle and different fixation protocols (Raemaekers et al., 2003).

We next analyzed whether the lack of NuSAP at the mitotic spindle was caused by reduced protein levels of NuSAP in metaphase of Misu-depleted cells. Protein levels of NuSAP were comparable in Scr RNAi and Misu RNAi cells synchronized in M phase of the cell cycle (Fig. 9 I). Interestingly, the localization of none of the spindle assembly factors, including NuSAP, to the spindle was dependent on RNA (Fig. S5, H–O), indicating that Misu does not mediate the binding of NuSAP to microtubules but instead might be required for the recruitment of NuSAP from the nucleoli to the spindle at the onset of mitosis.

We confirmed the interaction of NuSAP with Misu by reciprocal co-IP experiments (Fig. 9, J and K). Misu is not a direct target of the importin-α and -β dimer, as no interactions were observed by co-IP (Fig. 9 J). Similarly, Misu does not appear to interact with other spindle assembly factors (unpublished data).

NuSAP is a direct target gene of c-Myc

NuSAP shares a very similar pattern of cellular localization with Misu: it localizes to nucleoli during interphase and the spindle fibers during mitosis (Fig. 9, A–F). Furthermore, depletion of NuSAP by siRNA results in severe proliferation and metaphase defects, including abnormal spindle morphology and misalignment of chromosomes (Raemaekers et al., 2003). Given the similarities between NuSAP and Misu, we asked whether expression of NuSAP, like Misu, is regulated by c-Myc.

Published July 13, 2009

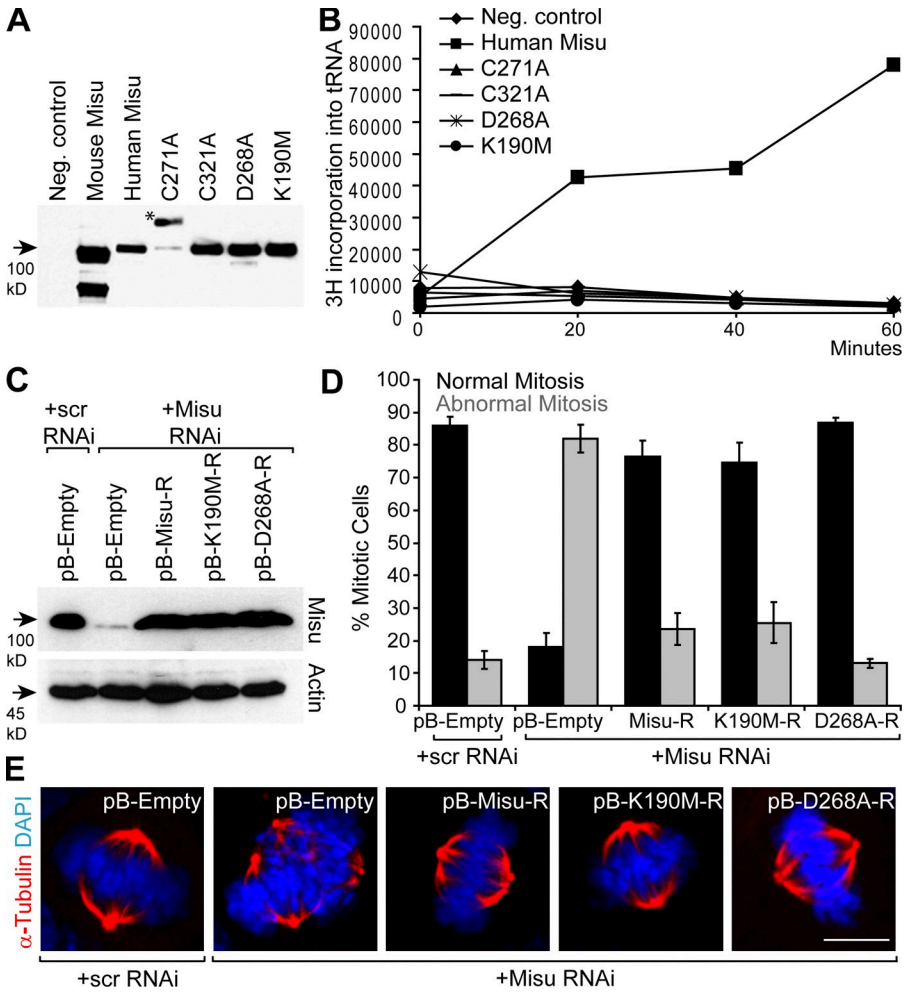

Figure 8. **The function of Misu at the spindle is independent from its methyltransferase activity.** (A) Western blot showing similar protein levels of wild-type Misu (mouse and human) as well as mutant constructs C271A, C321A, D268A, and K190M after purification. Lysates from uninfected cells served as negative control. The asterisk marks a shift in molecular mass in C271A. (B) Human Misu but none of the mutant constructs methylate tRNA in vitro. (C) Western blot showing Misu expression in Scr or Misu RNAi cells coinfected with empty vector control (pB-Empty) or rescue constructs pB-Misu-R, pB-K190M-R, and pB-D268A-R. (D) Quantification of mitotic defects (abnormal spindle) in Misu RNAi cells coinfected with pB-Empty or rescue constructs. Note that all RNAi-resistant constructs rescue defects in spindle morphology (normal mitosis) in the presence of Misu RNAi. Abnormal spindle structure, misaligned chromosomes, or multipolar spindles (Fig. 3) are grouped as abnormal mitosis. (E) Immunofluorescence for tubulin (red) and DAPI (blue) of cells quantified in D. Error bars indicate mean ± SD. Bar, 10 µm.

To analyze whether NuSAP was up-regulated in response to activated c-Myc, we performed quantitative real-time PCR (QPCR) using the epidermis of transgenic mice in which an inducible construct of c-Myc (MycER) is expressed (Arnold and Watt, 2001). In these transgenic mice, c-Myc can be activated by topical application of 4-hydroxytamoxifen (4-OHT). RNA expression of both Misu and NuSAP was increased when c-Myc was activated for 6 or 12 d with 4-OHT compared with wild-type littermates (Fig. 9, M and N). We identified five putative Myc-binding sites in the promoter region of NuSAP using the transcription element search system (Schug, 2008), suggesting that NuSAP may be a direct transcriptional target of c-Myc and thus contribute to c-Myc–driven proliferation.

To test whether c-Myc binds the promoter of NuSAP, we performed chromatin IP (ChIP) using the back skin of wild-type and MycER transgenic mice (Fig. 9 L). QPCR demonstrated that the NuSAP promoter was ∼30-fold enriched in cells derived from transgenic mice compared with wild-type mice in two independent biological replicates (Fig. 9 L, NuSAP). We confirmed that the nucleolin promoter, a well-known Myc target gene, was enriched in c-Myc binding (Fig. 9 L; Greasley et al., 2000) and that a genomic sequence 7 kb downstream of the nucleolin promoter was not bound (Fig. 9 L, control). Because Myc binds to the NuSAP promoter and drives NuSAP expression, we conclude that NuSAP is a novel transcriptional target gene of c-Myc.

Discussion

In this study, we provide evidence that Misu has a dual role in mammalian cells. In interphase of the cell cycle, Misu functions as a nucleolar RNA methyltransferase to ensure translation efficiency (Agris, 1996, 2004; Grosjean, 2005; Frye and Watt, 2006). During cell divisions, Misu and its bound RNA are required for proper spindle formation and integrity. The concept that protein complexes and their bound RNA molecules not only localize to the spindle but also play an essential role in mitotic microtubule assembly was first shown using *Xenopus* egg extracts (Blower et al., 2005). In *Drosophila melanogaster*, two RNA-associated proteins have been identified to be essential for mitotic spindle assembly: Hel25E (an RNA helicase) and Hrb27 (a RNP; Goshima et al., 2007). In yeast, the nucleolar protein Rrp14p associates with preribosomes and plays a role in correct positioning of the spindle during mitosis (Oeffinger et al., 2007). Collectively, these data indicate a complex yet evolutionary conserved role for RNAs and their protein-binding partners in regulating the balance between microtubule assembly and spindle organization.

Published July 13, 2009

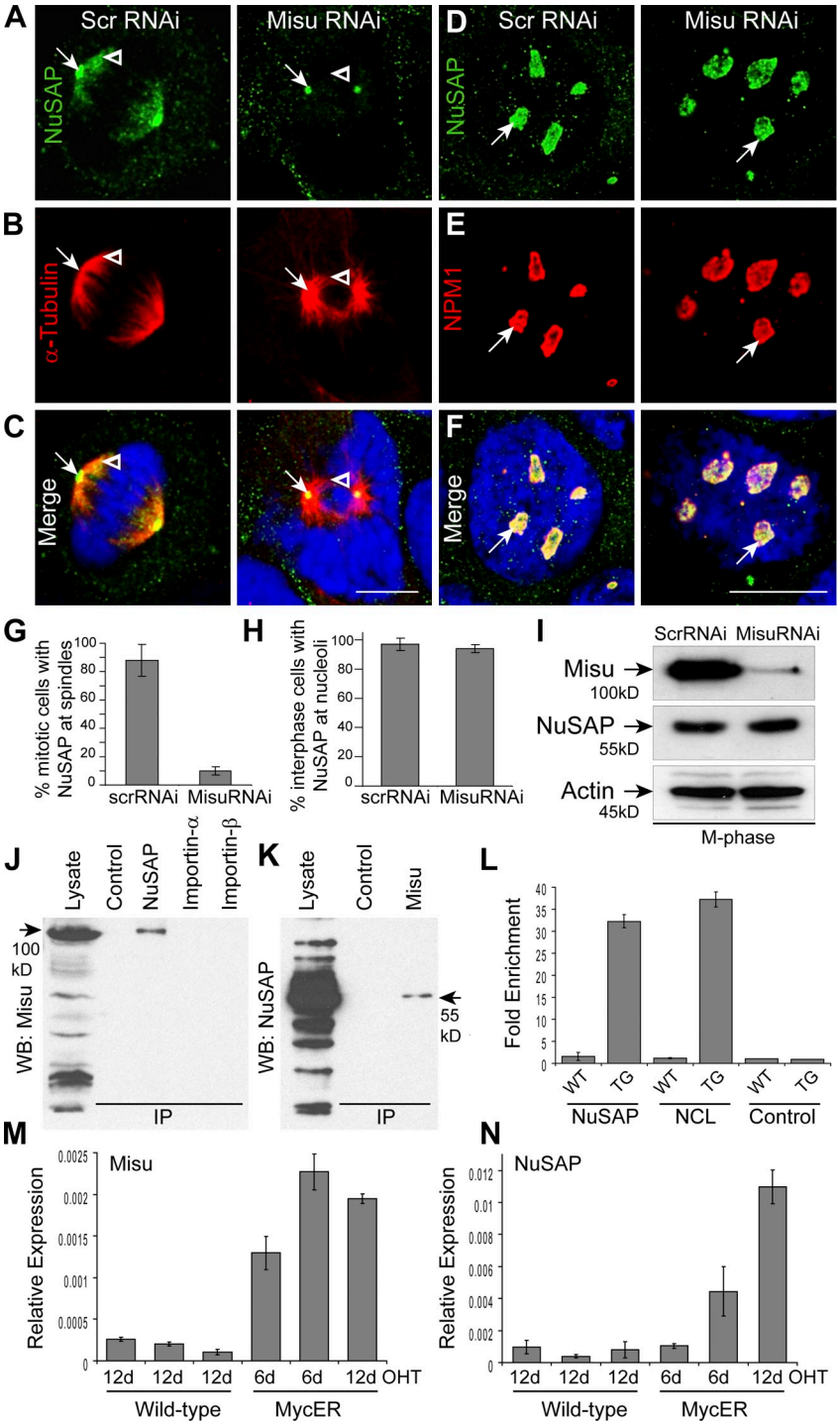

Figure 9. **Interaction of Misu and NuSAP is required for localization of NuSAP to the spindle and identification of NuSAP as direct target gene of c-Myc.** (A–C) In metaphase of control cells (Scr RNAi), NuSAP (green) colocalizes with α-tubulin (red) to the spindle (arrowheads) and spindle poles (arrows). (right) NuSAP staining at the spindle but not spindle poles is lost in Misu RNAi cells. (D–F) Colocalization of NuSAP with NPM1 at the nucleoli (arrows) is not affected in Misu RNAi cells. DNA is counterstained with DAPI (blue). (G and H) Quantification of A–F. (I) Western blot showing protein levels of NuSAP and Misu in Scr RNAi and Misu RNAi cells synchronized in M phase of the cell cycle. Actin served as loading control. (J and K) Reciprocal co-IP of Misu and NuSAP in HCC1954 cells. (J) NuSAP but not importin-α or -β co-IP with Misu. Preimmunoserum served as negative control (control). WB, Western blot. Arrows mark the size of the indicated proteins. (L) ChIP for NuSAP and nucleolin (NCL) promoters using Myc antibody in epidermis of transgenic (TG) and wild-type (WT) mice. Nucleolin promoters served as positive control, and genomic DNA downstream of the nucleolin promoter served as negative control. Values are normalized to whole cell lysates. (M and N) RNA levels of Misu (M) and NuSAP (N) are elevated in epidermis of Myc-overexpressing transgenic (MycER) but not wild-type mice in response to 4-OHT. Days of treatment are indicated on the x axis. Error bars indicate mean ± SD. Bars, 10 μm.

Our observation that depletion of Misu has multiple adverse effects on spindle integrity is consistent with our finding that Misu localizes to spindle poles and fibers. Some of the phenotypes resulting from Misu depletion, such as unstructured spindle fibers and misaligned metaphase chromosomes, were strikingly similar to those observed in response to RNaseA treatment. The localization of Misu at the spindle was dependent on the presence of RNA, indicating that a protein–RNA complex containing Misu and 18S rRNA contributes toward maintenance of mitotic spindle integrity. Misu might have additional roles during mitosis independent of RNA, as Misu localization to the spindle poles was not dependent on the presence of RNA.

In *Xenopus*, spindle-associated RNA is part of large RNP complexes. These complexes include Rae1 and several mRNA-associated proteins that have been implicated in various steps of mRNA biogenesis (Blower et al., 2005). Consequently, even certain conserved mRNA species associate with mitotic microtubules (Blower et al., 2007). Indeed, translation of mRNAs, encoding for proteins with functions in spindle assembly and chromosome segregation, occurs at the spindle and is essential

Published July 13, 2009

for proper meiotic division in *Xenopus* oocytes (Eliscovich et al., 2008). Although these data implied a translational role of Misu at the spindle, active translation was not required for the localization of Misu or 18S rRNA to mitotic microtubules. In addition, the methyltransferase activity of Misu was not required for its role in regulating spindle stability. Our results are consistent with a previously proposed translation-independent role of microtubule-associated RNAs in spindle assembly (Blower et al., 2005). Our data are further supported by the finding that phosphorylation of Misu by aurora B kinase leads to inhibition of its methyltransferase activity during mitosis (Sakita-Suto et al., 2007). Our data would predict a model in which aurora B kinase phosphorylates Misu, thereby regulating the function of Misu and its RNA-binding partner, 18S rRNA, on mitotic spindle assembly.

To understand how Misu mechanistically regulates spindle stability, we considered the possibility that Misu might interact with spindle assembly factors. One important pathway to form a spindle in mitosis involves the small nuclear GTPase Ran (Clarke and Zhang, 2008). The generation of Ran-GTP at chromosomes provides a spatial signal that directs microtubule reorganization through the release of spindle assembly factors from the inhibitory complexes with importins (Clarke and Zhang, 2008). One mitotic Ran-GTP target is NuSAP, an essential microtubule-stabilizing and -bundling protein (Raemaekers et al., 2003; Ribbeck et al., 2006).

Two possible explanations exist for the failure of NuSAP to localize to spindle fibers in Misu-depleted cells. Misu could be directly required for the binding of NuSAP to microtubules, or Misu may be required to actively relocate NuSAP to microtubules from the nucleoli at the onset of mitosis when the nucleolar architecture breaks down. Because NuSAP can bind directly to microtubules (Raemaekers et al., 2003; Ribbeck et al., 2006) and removal of Misu from the spindle via RNase did not affect the localization of NuSAP (Fig. S5, N and O), it is highly unlikely that Misu is required for the physical interaction of NuSAP with microtubules. Instead, we propose a model in which a Misu–NuSAP complex is required to relocate from the nucleolus to the spindle at the onset of mitosis.

Sequestering NuSAP and Misu in the nucleolus in interphase cells may provide a mechanism to prevent inappropriate activation of factors involved in regulating mitosis. It may be possible that phosphorylation of Misu by the aurora B kinase at the onset of mitosis acts as a signal for release and translocation of the Misu–NuSAP complex from the nucleolus to the spindle. This hypothesis is supported by the fact that phosphorylation of Misu by aurora B also causes Misu to dissociate from the nucleolar protein NPM1 (Sakita-Suto et al., 2007).

Although the localization of Misu to the spindle is strictly dependent on the presence of RNA, the localization of NuSAP at mitotic microtubules is not affected by RNase treatment (Fig. 6, F and G; and Fig. S5, N and O). Therefore, it is likely that NuSAP and Misu interact with the spindle via distinct mechanisms. Misu/Nsun2 is phosphorylated on multiple sites during mitosis (Dephoure et al., 2008), and many kinases are known to be localized at the spindle (Schmit and Ahmad, 2007; Dephoure et al., 2008; Taylor and Peters, 2008). Thus, it might be possible that phosphorylation of Misu at mitotic microtubules causes it to dissociate from NuSAP. Further investigation into the phosphorylation of Misu during mitosis should lead to a better understanding of its roles in cell division.

It is very likely that the observed spindle assembly defects in response to Misu RNAi are at least in part caused by the lack of NuSAP at the spindle. Several aspects of mitotic spindle formation are impaired when NuSAP is depleted, including the formation of stable mitotic spindles and chromosome segregation (Raemaekers et al., 2003). In addition to their function at the spindle, Misu and NuSAP share expression and cellular localization patterns. Expression of both proteins is restricted to proliferating cells, and to the best of our knowledge, NuSAP and Misu are the only two nonribosomal proteins identified so far to localize to both the nucleoli and mitotic spindle fibers (Raemaekers et al., 2003; Frye and Watt, 2006). The finding that both genes are direct target genes of c-Myc suggests that c-Myc can enable proliferation by up-regulating factors that stabilize mitotic microtubules in fast-dividing cells such as cancer cells.

Materials and methods

Cell culture

HCC1954 cells were cultured in DME (Invitrogen) supplemented with 10% FCS and Cal51, BT20, MT3, PMC42, and T47D cells in RPMI (Invitrogen) supplemented with 10% FCS in a humidified atmosphere at 37°C and 5% CO_2. T47D cells were also supplemented with 5 µg/ml insulin.

RNAi knockdown and retroviral infection

Cells were infected with the retroviral vector pRS. The oligonucleotide that gave optimal knockdown of Misu was RNAi, 5′-GAGATCCTCTTCTATGATC-3′ (Frye and Watt, 2006). The Misu RNAi oligonucleotide was used in all experiments along with an Scr construct, 5′-GTACTGCTTACGATACGGA-3′. For RNAi rescue experiments, two silent mutations were introduced in the RNAi target sequence of wild-type Misu and K190M and D268A mutant constructs using the site-directed mutagenesis kit (Agilent Technologies). These constructs were retrovirally infected using pBabe (pB-Misu-R, pB-K190M-R, and pB-D268A-R). The primers used for mutagenesis were (forward) 5′-GGCAGGAAAGAGATCCTaTTtTATGATCGAATTTTATGT-3′ and (reverse) 5′-ACATAAAATTCGATCATAaAAtAGGATCTCTTTCCTGCC-3′. Lowercase letters refer to mutated residues. For HCC1954 infection, the constructs were transfected by calcium phosphate precipitation into Phoenix-E retrovirus-producer cells. After 2 d, the supernatant of Phoenix-E cells was transferred onto retrovirus-packaging AM12 cells for 2 d. Mitomycin-treated AM12 cells were cocultured with HCC1954 cells in a ratio of 1:4 for 24 h and selected with puromycin for 2 d. After 3 d, the HCC1954 cells outgrow the AM12, and the culture consists of 95–100% HCC1954 cells. Infected HCC1954 cells were used for experiments either immediately or after one cell passage. For RNAi rescue experiments, coinfections were performed by initially generating individual AM12 lines that express either the pRS knockdown or pBabe rescue constructs. HCC1954 cells were coinfected by coculturing them with the appropriate AM12 cells at a 1:1:6 ratio of pRS knockdown AM12/pBabe rescue AM12/HCC1954.

siRNA knockdown and cell synchronization

HCC1954 and Cal51 cells were synchronized in G1 phase of the cell cycle using serum starvation for a period of 72 h. To synchronize cells in M phase, cells were treated with 10 mM thymidine (Sigma-Aldrich) for 15 h followed by a 9-h release. A second 10-mM thymidine block was performed for a further 15 h followed by a 5-h release. Cells were arrested in M phase using 40 ng/ml nocodazole (Sigma-Aldrich) for 8 h. Microtubule assembly was allowed to proceed by culturing cells in drug-free medium for 45 min, at which point cells were harvested or fixed for further analysis. In some experiments, within the first 2 h of the 9-h release period after the first thymidine block, cells were transfected with control or Misu siRNA (QIAGEN) using HiPerFect transfection reagent (QIAGEN) according to the manufacturer's instructions. The Misu siRNA consisted of the sequence 5′-CACGTGTTCACTAAACCCTAT-3′. As negative control, the AllStars negative control siRNA (QIAGEN) was used.

Published July 13, 2009

Immunofluorescence staining and image acquisition

Cells were fixed and permeabilized in methanol for 10 min at −20°C and blocked with 5% FCS in PBS before antibody incubations. Alternatively, cells were preextracted with 0.1% Triton X-100 in microtubule stabilization PHEM buffer (60 mM Pipes, 25 mM Hepes, 10 mM EGTA, and 1 mM $MgCl_2$, pH 6.9) for 2 min before fixation with 4% paraformaldehyde in PBS and subsequent blocking with 5% FCS in PBS. Cells were incubated with primary antibody in blocking buffer. EF-1 and EF-2 rabbit polyclonal anti-Misu antibodies were used in this study (Frye and Watt, 2006). Other antibodies used were NPM1 (FC82291; Sigma-Aldrich), α-tubulin (DM1A; Sigma-Aldrich), importin-α (anti-Kpnα2; EMD), importin-β (anti-Kpnβ1; EMD), and phospho-γH2A.X (Millipore). Antibodies to TPX2, TACC3, and aurora A were provided by F. Gergely (Cancer Research UK, Cambridge, England, UK), and the antibodies for NuSAP were provided by G. Carmeliet (Katholieke Universiteit Leuven, Leuven, Belgium). Cells were incubated with appropriate fluorophore-conjugated secondary antibodies (Alexa Fluor 488, -532, and -568), and slides were mounted in Vectashield (Vector Laboratories). Images were obtained using a confocal microscope (SP5; Leica) with a HCX Plan Apo 63× 1.4 numerical aperture objective lens (Leica) at room temperature using oil immersion as imaging medium. Leica Application Suite Advanced Fluorescence acquisition software was used.

In some cases, cells were treated with 50 µg/ml puromycin for 45 min before methanol fixation to inhibit protein translation. For quantification of adverse effects of Misu RNAi and siRNA constructs, transduced HCC1954 cells were stained for α-tubulin and DAPI (see previous paragraph). Data were pooled from two independent experiments, and 200 mitotic cells were scored in total. 100 interphase cells were scored on the basis of how many nuclei they contained. Only cells that contained at least three nuclei were scored as polynucleated.

Fluorescent visualization of 18S rRNA

To visualize the cellular localization of 18S rRNA, a 50-nucleotide Alexa Fluor 488 fluorophore–labeled antisense DNA probe was designed. The probe consisted of the sequence 5′-CACCCGTGGTCACCATGGTAGGCACGGCGACTACCATCGAAAGTTGATAG-3′ and was synthesized and labeled by Invitrogen. Cells were fixed in methanol as described in the previous section. After methanol fixation, cells were incubated for 16–20 h in the dark at 4°C with 1 µM Alexa Fluor 488–18S rRNA probe in PBS. Cells were washed extensively in PBS, and slides were mounted in Vectashield. In some experiments, the 18S rRNA antisense probe was allowed to anneal to an exact complementary sense oligonucleotide before cell stainings by heating a 1:5 ratio of antisense probe/sense oligo mixture to 95°C and allowing the mixture to cool gradually to room temperature. In some experiments, mouse monoclonal α-tubulin antibody was coincubated with Alexa Fluor 488–18S rRNA probe followed by secondary antibody detection of α-tubulin antibody.

RNaseA treatments

RNaseA (Sigma-Aldrich) was boiled for 10 min to remove any DNase impurity and frozen in aliquots. RNaseA was used at a final concentration of 100 µg/ml in PBS. For immunofluorescence staining experiments, RNaseA was added to cells in between the preextraction and fixation steps (see Immunofluorescence staining and image aquisition) for a period of 15 min, or otherwise, cells were treated with PBS.

Co-IP and Western blotting

HCC1954 cells were lysed in lysis buffer (1% NP-40, 200 mM NaCl, 25 mM Tris-HCl, pH 8, 1 mM DTT, and protease inhibitor cocktail) for 30 min on ice. Lysates were cleared by centrifugation at 13,000 rpm and divided equally between each IP reaction. For each IP, 0.5 ml lysate was diluted 1:10 in IP buffer (200 mM NaCl, 25 mM Tris-HCl, pH 8, 1 mM DTT, 10% glycerol, and protease inhibitor cocktail) with protein A agarose beads and the appropriate antibody. IPs were incubated for 16 h at 4°C with gentle mixing. After five 10 ml washes with IP buffer, beads were resuspended in SDS protein sample buffer, and samples were electrophoresed on a 10% SDS polyacrylamide gel. Gels were blotted onto polyvinylidene difluoride membranes, which were incubated in TBST-blocking solution (Tris-buffered saline, pH 8.8, with 5% marvel milk powder). Blots were incubated with primary antibodies in blocking solution followed by incubation with the appropriate HRP-conjugated secondary antibodies. The chemiluminescent signal was detected using an ECL chemiluminescent kit (GE Healthcare) according to the manufacturer's instructions. Alternatively, Western blotting was performed using the One-Step IP-Western kit (GenScript Corporation) according to the manufacturer's instructions.

Identification of Misu-associated RNAs

To identify RNAs that interact with Misu, IPs were performed as described in the previous section except that lysis was performed in the presence of 0.5% NP-40 instead of 1% NP-40. Immunoprecipitated agarose beads were resuspended in SDS sample buffer, and samples were electrophoresed on ethidium bromide–stained 1% agarose gels. Some immunoprecipitated samples were treated with 100 µg/ml RNaseA for 15 min just before addition of SDS sample buffer. RNA bands were gel purified using an RNeasy Mini kit (QIAGEN). To confirm the identity of 18S rRNA, RT-PCR analysis was used. Reverse transcription was performed using Superscript II reverse transcription (Invitrogen) with the 5′-ACGGAATCGAGAAAGAGCTATCAATCTGTC-3′ primer specific for 18S rRNA. 25 cycles of PCR were performed with *Thermococcus kodakaraensis* polymerase (EMD) to amplify a 724-bp region (571–1,294 bp; GenBank accession no. M10098) of 18S rRNA using the primers (forward) 5′-GGCAGCAGGCGCGCAAATTACCCAC-3′ and (reverse) 5′-AAGTTTCAGCTTTGCAACCATACTC-3′. To detect 5S and 5.8S rRNA, RT-PCR was performed either directly on washed IP samples or on whole cell lysate as a positive control. The primer used for reverse transcription of 5S rRNA was 5′-AAAGCCTACAGCACCCGGTATTCCCAG-3′, and the PCR primers used were (forward) 5′-GTCTACGGCCATACCACCCTGAACG-3′ and (reverse) 5′-AAAGCCTACAGCACCCGGTATTCCCAG-3′. The primer used for reverse transcription of 5.8S rRNA was 5′-AAGCGACGCTCAGACAGGCGTAGC-3′, and the PCR primers used were (forward) 5′-CGACTCTTAGCGGTGGATCACTCG-3′ and (reverse) 5′-AAGCGACGCTCAGACAGGCGTAGC-3′.

FACS analysis

To quantify apoptosis, the polycaspase fluorochrome inhibitor of caspases (FLICA) apoptosis detection kit was used as per the manufacturer's instructions (Immunochemistry Technologies). FLICA probe, which covalently binds to activated caspases, was incubated with cells for 1 h, and cells were washed extensively in wash buffer before FACS analysis was performed on an ADP analyzer (CyAn; Dako). As a positive control, cells were treated with 500 ng/ml actinomycin D for 4 h before FACS analysis to induce apoptosis. For quantification of necrosis, cells were stained with 2.5 µg/ml propidium iodide for 15 min before FACS analysis.

Quantification of micronuclei

Nuclei were stained with DAPI, and ImageJ software (National Institutes of Health) was used to computationally quantify micronuclei. Random areas of the slide were tile scanned using an inverted microscope (DMI4000B; Leica) with an A4 filter and 20× objective, and the images were analyzed using ImageJ. The images were deblurred by subtraction of a Gaussian blur (radius of 20 pixels) and thresholded to delineate nuclei. Micronuclei of ≤120 μm^2 were observed, and this size was set as the upper boundary to delineate micronuclei. Micronuclei with a size as low as 20 μm^2 were also typically observed, and to minimize the likelihood of scoring artifactual particles, DAPI-stained material <20 μm^2 was excluded from the analysis. 6,000 nuclei were scored for each sample.

Protein expression, purification, and in vitro methylation assay

Full-length human Misu was purchased from OriGene and subcloned into pFastBac HT vector with 6×His N-terminal epitope tag. Four mutant constructs (D268A, C271A, C321A, and K190M) were generated using the site-directed mutagenesis kit (QuikChange XL; Agilent Technologies) according to the manufacturer's instructions using the following primers: D268A, (forward) 5′-TATGATCGAATTTTATGTGCTGTCCCTTGCAGTGGAGAC-3′ and (reverse) 5′-GTCTCCACTGCAAGGGACAGCACATAAAATTCGATCATA-3′; C271A, (forward) 5′-AATTTTATGTGATGTCCCTGCCAGTGGAGACGGCACTATG-3′ and (reverse) 5′-CATAGTGCCGTCTCCACTGGCAGGGACATCACATAAAATT-3′; C321A, (forward) 5′-AAGGATGGTGTATTCCACGGCTTCACTAAACCCTATTGAG-3′ and (reverse) 5′-CTCAATAGGGTTTAGTGAAGCCGTGGAATACACCATCCTT; and K190M, (forward) 5′-TGCAGCACCTGGCTCAATGACCACACAGTTAATTG-3′ and (reverse) 5′-CAATTAACTGTGTGGTCATTGAGCCAGGTGCTGCA-3′.

25 ml of Sf9 insect cells was infected with baculovirus (MOI = 5). 3 d later, cells were centrifuged, and pellets were processed for protein purification. Cell lysis was performed with 1 ml CytoBuster protein extraction reagent (EMD). The lysate was diluted to 2 ml with binding buffer (50 mM sodium phosphate buffer, pH 8.0, 300 mM NaCl, and 20 mM imidazole) and clarified by centrifugation at full speed for 5 min at 4°C. Supernatants were purified on His SpinTrap affinity columns (GE Healthcare) following the manual's instructions and eluted with 500 mM imidazole. Proteins were stored at −80°C in 30% glycerol.

Published July 13, 2009

Methylation assays were performed using 1 µg of each purified protein or negative control (purification from uninfected Sf9 cells), 10 µg tRNA from *E. coli* (Sigma-Aldrich), and 0.20 µM S-Adenosyl-L-[methyl-^{3}H]methionine (GE Healthcare). The total reaction volume of 120 µl was buffered with 100 mM MOPS, pH 7.8, 100 mM ammonium acetate, 1 mM magnesium acetate, 5 mM DTT, and 6 U RNasin. Reactions were incubated at 30°C, and 25 µl of mixture was placed in 1 ml cold 5% TCA at each time point. Each sample was vacuum filtered though a 25-mm GF/C filter (GE Healthcare) and washed five times with 2 ml 5% TCA and twice with 2 ml 96% ethanol to eliminate unincorporated radioactivity. Filters were left to dry. The amount of radiolabel incorporated into RNA was determined by placing the filters in 5 ml of scintillation fluid and counting in a scintillation counter (Beckman Coulter).

Transgenic mice and QPCR

All mouse husbandry and experimental procedures were conducted in compliance with the protocols established by the local ethics committee under the terms of a UK Home Office license. K14MycER transgenic mice (2184C.1) received topical applications of 4-OHT (1 mg/0.2 ml ethanol; 1 mg/mouse/day) to a shaved area of dorsal skin (Arnold and Watt, 2001).

RNA from transgenic and wild-type littermate controls was isolated from total skin (epidermis plus dermis). Total RNA was prepared using Trizol reagent (Invitrogen) according to the manufacturer's instructions. Double-stranded cDNA was generated from 1 µg total RNA using an RNA to cDNA kit (Applied Biosystems) following the manufacturer's protocols. PCR amplification was performed in triplicate of each first-strand cDNA plus primer and probe master mix containing 1 µl cDNA, 5 µl TaqMan Fast Universal PCR Master Mix (2×), No AmpErase UNG, with 0.5 µl TaqMan probes for Misu (Mm00520224_m1), and NuSAP (Mm00505602_m1). Glyceraldehyde 3-phosphate dehydrogenase control reagent (VIC probe; Applied Biosystems) was used according to the manufacturer's instructions. real-time PCR reactions and analysis were performed with a real-time PCR system (7900HT; Applied Biosystems). The relative amount of each mRNA was normalized to the level of glyceraldehyde 3-phosphate dehydrogenase in each sample.

ChIP and QPCR

Primary mouse keratinocytes were isolated from 4-OHT–treated dorsal skin of transgenic and nontransgenic mice. Back skin of six mice each was pooled and used for one ChIP experiment. The shaved and treated skin was cut and washed in 10% betadine solution, 70% ethanol, and twice in PBS. The tissue was trypsinized for 2 h at 37°C. The epidermis was cut into small pieces, and cell suspensions were filtered through a cell strainer. After centrifugation, mouse keratinocytes were fixed in 1% formaldehyde for 20 min at room temperature. Cross-linking was terminated by addition of 2.5 M glycine for 10 min.

Mouse keratinocytes were incubated for 10 min at 4°C in 10 ml of lysis buffer 1 (50 mM Hepes-KOH, pH 7.5, 140 mM NaCl, 1 mM EDTA, 10% glycerol, 0.5% NP-40, and 0.25% Triton X-100), 10 ml of lysis buffer 2 (200 mM NaCl, 1 mM EDTA, 0.5 mM EGTA, and 10 mM Tris, pH 7.5), and 5 min at 4°C in 3 ml of lysis buffer 3 (1 mM EDTA, 0.5 mM EGTA, 10 mM Tris-HCl, pH 7.5, 0.1% Na-deoxycholate, and 0.5% *N*-lauroyl sarcosine) containing protease inhibitor cocktail tablets (Complete mini EDTA free; Roche). Cells were sonicated using an automatic sonicator (3000; Misonix). A first cycle of 12 pulses of 30 s was applied with an output of 30 W followed by a second cycle of four pulses of 30 s under the same conditions. Cells were kept in an ice water bath during sonication and cooled for 1 min between pulses. Cell extracts were diluted in a 1:10 vol of 10% Triton X-100 solution. 50 µl of the supernatant of the whole cell extract (WCE) material was diluted in 150 µl of elution buffer (50 mM Tris, pH 8, 1 mM EDTA, and 1% SDS) and stored at −20°C. The remaining sample was used for IP.

Sonicated fractions were incubated with 100 µl antibody (20 µg c-Myc antibody; sc-N262) prebound to streptavidin magnetic beads (Dynabeads M-270 streptavidin; Invitrogen) at 4°C overnight. The DNA–protein complexes were eluted in 200 µl of elution buffer by incubation at 65°C for 10–15 min with brief vortexing every 2 min. The IP and WCE samples were reverse cross-linked at 65°C overnight. DNA from WCE and IP samples was isolated using phenol chloroform extraction.

DNA was subjected to blunt end filling using Klenow and purified using DNA Clean & Concentrator-5 (Zymo Research, USA) according to the manufacturer's instructions. After linker ligation (5′-G*CGGTGACCCGGGAGATCTGAATTCT-3′ and 5′-G*AATTCAGATC-3′, asterisks indicate phosphorothioate), samples were amplified by PCR (5′-GCGGTGACCCGGGAGATCTGAATTC-3′). DNA was purified using a QiAquick PCR purification kit (QIAGEN) following the manufacturer's protocol. The DNA concentration was normalized to 100 ng/µl using a spectrophotometer (ND-1000; Nanodrop Technologies). ChIP experiments with mouse keratinocytes were performed in replicate.

QPCR was performed using SYBR green. In brief, 2 µl IP DNA was diluted to a 20-µl QPCR reaction containing 12.5 µl Fast SYBR green (2×; Applied Biosystems), 0.6 µl forward and reverse primers (6 µM), and 12 µl of ultrapure water. Primers to amplify genomic DNA surrounding the Myc-binding sites were as follows: nucleolin, (forward) 5′-GGCTGGAAGCGAGAGAAAG-3′ and (reverse) 5′-TCACCTCTTAAAGCAGCACCA-3′; and NuSAP, (forward) 5′-CCTTCAGGTTTTTGCTATCTTCTC-3′ and (reverse) 5′-CAGGATAGCCCAGGCAGTAT-3′. As a negative control, a DNA region of ∼7,000 bp downstream the Myc-binding sites was amplified: negative control, (forward) 5′-GCTGGCCTCAAACTCAGAAA-3′ and (reverse) 5′-GGCGCACACCTTTAATCC-3′. Enrichment of Myc binding in promoter regions was quantified by normalization to the WCE of each sample.

Online supplemental material

Fig. S1 shows that ectopically expressed Misu localizes to the spindle in T47D cells and confirms localization of Misu at the spindle using EF2 antibody. Fig. S2 confirms Misu repression in response to Misu RNAi/siRNA and demonstrates that all tested cancer cell lines exhibit mitotic defects upon removal of Misu. Fig. S3 shows that depletion of Misu does not result in DNA double-strand breaks. It further confirms the specificity of the 18S rRNA probe and shows colocalization of Misu and 18S rRNA in HCC1954 cells. Fig. S4 shows that 18S rRNA localization to the spindle is not affected by depletion of Misu, and localization of Misu to the spindle is independent of active translation. It also shows cellular localization of NuSAP in metaphase and anaphase of the cell cycle using different fixation methods. Fig. S5 shows that depletion of Misu does not affect cellular localization of aurora A, TPX2, and TACC3 to the spindle. All spindle assembly factors, including NuSAP, localize to the spindle when cells are treated with RNaseA. Online supplemental material is available at http://www.jcb.org/cgi/content/full/jcb.200810180/DC1.

We are most grateful to Geert Carmeliet, An Vanden Bosch, Werner Verbakel, and Fanni Gergely for reagents, advice, and very helpful comments on this manuscript. We also thank Fiona Watt, Nigel Miller, Duncan Odom, and Salvador Aznar-Benitah for providing us with advice and reagents.

This work was funded by Cancer Research UK. S.B. Benavente was supported by the Ramón Areces Spanish Foundation and the European Molecular Biology Organization. Misu is part of a current patent application.

Submitted: 29 October 2008
Accepted: 12 June 2009

References

Agris, P.F. 1996. The importance of being modified: roles of modified nucleosides and Mg2+ in RNA structure and function. *Prog. Nucleic Acid Res. Mol. Biol.* 53:79–129.

Agris, P.F. 2004. Decoding the genome: a modified view. *Nucleic Acids Res.* 32:223–238.

Albee, A.J., W. Tao, and C. Wiese. 2006. Phosphorylation of maskin by Aurora-A is regulated by RanGTP and importin beta. *J. Biol. Chem.* 281:38293–38301.

Andersen, J.S., Y.W. Lam, A.K. Leung, S.E. Ong, C.E. Lyon, A.I. Lamond, and M. Mann. 2005. Nucleolar proteome dynamics. *Nature.* 433:77–83.

Andrews, P.D., E. Knatko, W.J. Moore, and J.R. Swedlow. 2003. Mitotic mechanics: the auroras come into view. *Curr. Opin. Cell Biol.* 15:672–683.

Arnold, I., and F.M. Watt. 2001. c-Myc activation in transgenic mouse epidermis results in mobilization of stem cells and differentiation of their progeny. *Curr. Biol.* 11:558–568.

Blower, M.D., M. Nachury, R. Heald, and K. Weis. 2005. A Rae1-containing ribonucleoprotein complex is required for mitotic spindle assembly. *Cell.* 121:223–234.

Blower, M.D., E. Feric, K. Weis, and R. Heald. 2007. Genome-wide analysis demonstrates conserved localization of messenger RNAs to mitotic microtubules. *J. Cell Biol.* 179:1365–1373.

Boisvert, F.M., S. van Koningsbruggen, J. Navascues, and A.I. Lamond. 2007. The multifunctional nucleolus. *Nat. Rev. Mol. Cell Biol.* 8:574–585.

Brzezicha, B., M. Schmidt, I. Makalowska, A. Jarmolowski, J. Pienkowska, and Z. Szweykowska-Kulinska. 2006. Identification of human tRNA:m5C methyltransferase catalysing intron-dependent m5C formation in the first position of the anticodon of the pre-tRNA Leu (CAA). *Nucleic Acids Res.* 34:6034–6043.

Bujnicki, J.M., M. Feder, C.L. Ayres, and K.L. Redman. 2004. Sequence-structure-function studies of tRNA:m5C methyltransferase Trm4p and its relationship to DNA:m5C and RNA:m5U methyltransferases. *Nucleic Acids Res.* 32:2453–2463.

Clarke, P.R., and C. Zhang. 2008. Spatial and temporal coordination of mitosis by Ran GTPase. *Nat. Rev. Mol. Cell Biol.* 9:464–477.

Dephoure, N., C. Zhou, J. Villen, S.A. Beausoleil, C.E. Bakalarski, S.J. Elledge, and S.P. Gygi. 2008. A quantitative atlas of mitotic phosphorylation. *Proc. Natl. Acad. Sci. USA.* 105:10762–10767.

Eliscovich, C., I. Peset, I. Vernos, and R. Mendez. 2008. Spindle-localized CPE-mediated translation controls meiotic chromosome segregation. *Nat. Cell Biol.* 10:858–865.

Frye, M., and F.M. Watt. 2006. The RNA methyltransferase Misu (NSun2) mediates Myc-induced proliferation and is upregulated in tumors. *Curr. Biol.* 16:971–981.

Frye, M., C. Gardner, E.R. Li, I. Arnold, and F.M. Watt. 2003. Evidence that Myc activation depletes the epidermal stem cell compartment by modulating adhesive interactions with the local microenvironment. *Development.* 130:2793–2808.

Gautier, T., M. Robert-Nicoud, M.N. Guilly, and D. Hernandez-Verdun. 1992. Relocation of nucleolar proteins around chromosomes at mitosis. A study by confocal laser scanning microscopy. *J. Cell Sci.* 102:729–737.

Goshima, G., R. Wollman, S.S. Goodwin, N. Zhang, J.M. Scholey, R.D. Vale, and N. Stuurman. 2007. Genes required for mitotic spindle assembly in *Drosophila* S2 cells. *Science.* 316:417–421.

Greasley, P.J., C. Bonnard, and B. Amati. 2000. Myc induces the nucleolin and BN51 genes: possible implications in ribosome biogenesis. *Nucleic Acids Res.* 28:446–453.

Grosjean, H. 2005. Modification and editing of RNA: historical overview and important facts to remember. *In* Fine-Tuning of RNA Functions by Modification and Editing. Springer, Berlin/Heidelberg. 1–22.

Gruss, O.J., R.E. Carazo-Salas, C.A. Schatz, G. Guarguaglini, J. Kast, M. Wilm, N. Le Bot, I. Vernos, E. Karsenti, and I.W. Mattaj. 2001. Ran induces spindle assembly by reversing the inhibitory effect of importin alpha on TPX2 activity. *Cell.* 104:83–93.

King, M.Y., and K.L. Redman. 2002. RNA methyltransferases utilize two cysteine residues in the formation of 5-methylcytosine. *Biochemistry.* 41:11218–11225.

Liau, M.C., and R.B. Hurlbert. 1975. Interrelationships between synthesis and methylation of ribosomal RNA in isolated Novikoff tumor nucleoli. *Biochemistry.* 14:127–134.

Ma, N., S. Matsunaga, H. Takata, R. Ono-Maniwa, S. Uchiyama, and K. Fukui. 2007. Nucleolin functions in nucleolus formation and chromosome congression. *J. Cell Sci.* 120:2091–2105.

Nachury, M.V., T.J. Maresca, W.C. Salmon, C.M. Waterman-Storer, R. Heald, and K. Weis. 2001. Importin beta is a mitotic target of the small GTPase Ran in spindle assembly. *Cell.* 104:95–106.

Obara, M., K. Higashi, and Y. Kuchino. 1982. Isolation of nucleolar methylase producing only 5-methylcytidine in ribosomal RNA. *Biochem. Biophys. Res. Commun.* 104:241–246.

Oeffinger, M., A. Fatica, M.P. Rout, and D. Tollervey. 2007. Yeast Rrp14p is required for ribosomal subunit synthesis and for correct positioning of the mitotic spindle during mitosis. *Nucleic Acids Res.* 35:1354–1366.

Raemaekers, T., K. Ribbeck, J. Beaudouin, W. Annaert, M. Van Camp, I. Stockmans, N. Smets, R. Bouillon, J. Ellenberg, and G. Carmeliet. 2003. NuSAP, a novel microtubule-associated protein involved in mitotic spindle organization. *J. Cell Biol.* 162:1017–1029.

Ribbeck, K., A.C. Groen, R. Santarella, M.T. Bohnsack, T. Raemaekers, T. Kocher, M. Gentzel, D. Gorlich, M. Wilm, G. Carmeliet, et al. 2006. NuSAP, a mitotic RanGTP target that stabilizes and cross-links microtubules. *Mol. Biol. Cell.* 17:2646–2660.

Rogakou, E.P., D.R. Pilch, A.H. Orr, V.S. Ivanova, and W.M. Bonner. 1998. DNA double-stranded breaks induce histone H2AX phosphorylation on serine 139. *J. Biol. Chem.* 273:5858–5868.

Sakita-Suto, S., A. Kanda, F. Suzuki, S. Sato, T. Takata, and M. Tatsuka. 2007. Aurora-B regulates RNA methyltransferase NSUN2. *Mol. Biol. Cell.* 18:1107–1117.

Sato, M., and T. Toda. 2007. Alp7/TACC is a crucial target in Ran-GTPase-dependent spindle formation in fission yeast. *Nature.* 447:334–337.

Schmit, T.L., and N. Ahmad. 2007. Regulation of mitosis via mitotic kinases: new opportunities for cancer management. *Mol. Cancer Ther.* 6:1920–1931.

Schug, J. 2008. Using TESS to predict transcription factor binding sites in DNA sequence. *Curr. Protoc. Bioinformatics*. Chapter 2:Unit 2.6. John Wiley and Sons, Inc.

Taylor, S., and J.M. Peters. 2008. Polo and Aurora kinases: lessons derived from chemical biology. *Curr. Opin. Cell Biol.* 20:77–84.

Trieselmann, N., S. Armstrong, J. Rauw, and A. Wilde. 2003. Ran modulates spindle assembly by regulating a subset of TPX2 and Kid activities including Aurora A activation. *J. Cell Sci.* 116:4791–4798.

Tsai, M.Y., C. Wiese, K. Cao, O. Martin, P. Donovan, J. Ruderman, C. Prigent, and Y. Zheng. 2003. A Ran signalling pathway mediated by the mitotic kinase Aurora A in spindle assembly. *Nat. Cell Biol.* 5:242–248.

Tscherne, J.S., K. Nurse, P. Popienick, H. Michel, M. Sochacki, and J. Ofengand. 1999. Purification, cloning, and characterization of the 16S RNA m5C967 methyltransferase from *Escherichia coli*. *Biochemistry.* 38:1884–1892.

Waikel, R.L., Y. Kawachi, P.A. Waikel, X.J. Wang, and D.R. Roop. 2001. Deregulated expression of c-Myc depletes epidermal stem cells. *Nat. Genet.* 28:165–168.

Watt, F.M., M. Frye, and S.A. Benitah. 2008. MYC in mammalian epidermis: how can an oncogene stimulate differentiation? *Nat. Rev. Cancer.* 8:234–242.

Wiese, C., A. Wilde, M.S. Moore, S.A. Adam, A. Merdes, and Y. Zheng. 2001. Role of importin-beta in coupling Ran to downstream targets in microtubule assembly. *Science.* 291:653–656.

Wu, P., J.S. Brockenbrough, M.R. Paddy, and J.P. Aris. 1998. NCL1, a novel gene for a non-essential nuclear protein in *Saccharomyces cerevisiae*. *Gene.* 220:109–117.

Published July 13, 2009

Hussain et al., http://www.jcb.org/cgi/content/full/jcb.200810180/DC1

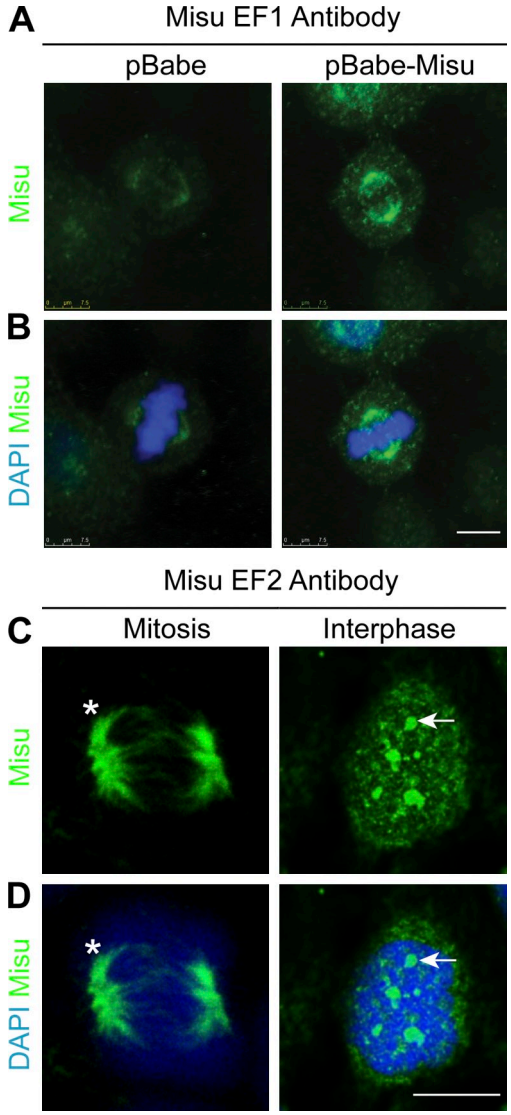

Figure S1. **Misu localizes to the spindle and the nucleoli.** (A) Expression of endogenous Misu (green) is weak at the spindle in T47D cells. (B) Overexpressed Misu (green) localized to mitotic microtubules. (C and D) EF2 antibody detects Misu (green) at the spindle in mitosis (asterisks) and the nucleoli in interphase (arrows). Cells are counterstained with DAPI (blue). Bars, 10 µm.

Published July 13, 2009

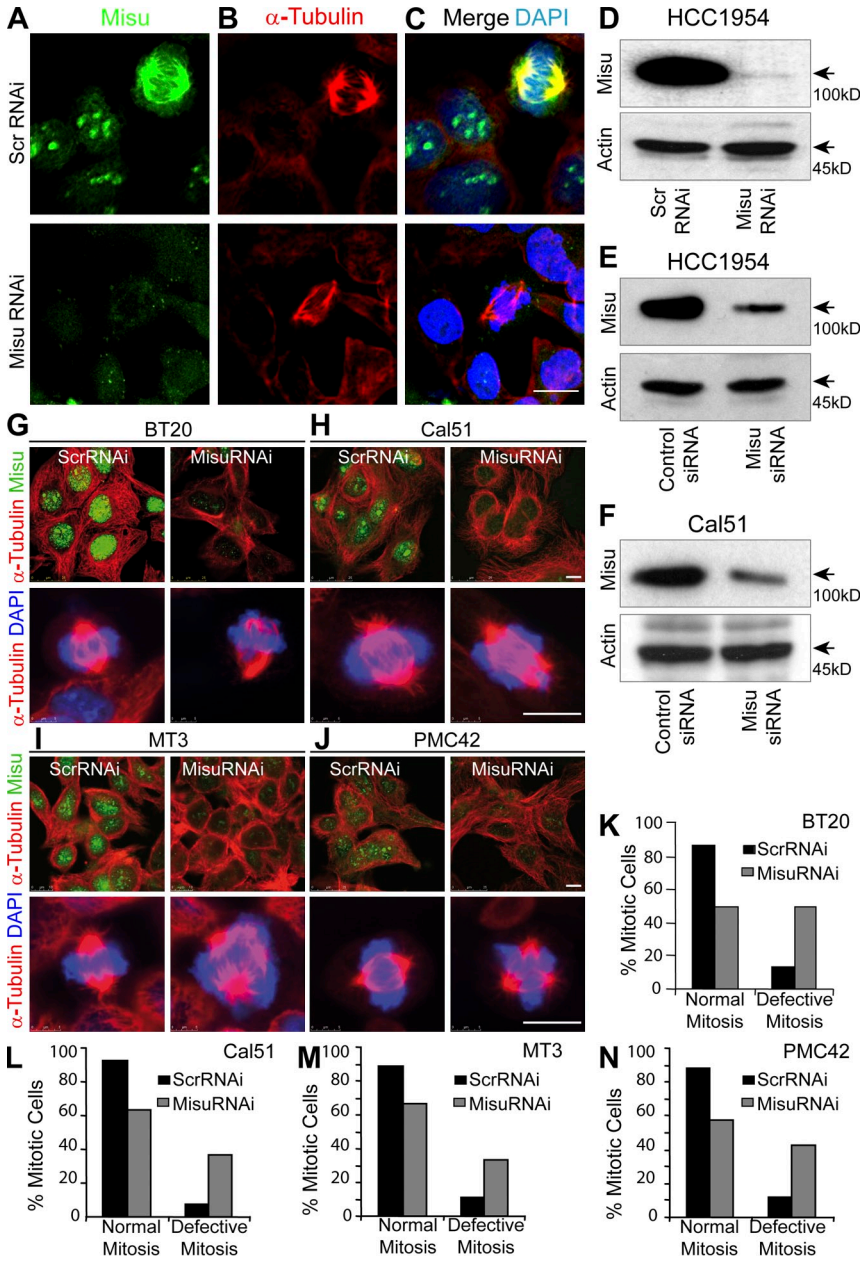

Figure S2. **Depletion of Misu expression using RNAi in different breast cancer cell lines results in defective mitosis.** (A–C) Misu (green) is absent from nucleoli and spindle fibers when cells are transduced with Misu RNAi but not when an Scr RNAi construct is used. Bar, 10 µm. (D–F) Western blots showing knockdown of Misu in response to Misu RNAi in HCC1954 cells (D), Misu siRNA in HCC1954 cells (E), and Misu siRNA in Cal51 cells (F). (G–J, top) Misu RNAi depletes Misu in BT20 (G), Cal51 (H), MT3 (I), and PMC42 (J) and causes mitotic defects (bottom). Spindles are visualized using α-tubulin antibody (red), and DNA is stained with DAPI (blue). Bars, 5 µm. (K–N) Quantification of mitotic defects from G–J. Data in K–N are representative of two experiments.

Published July 13, 2009

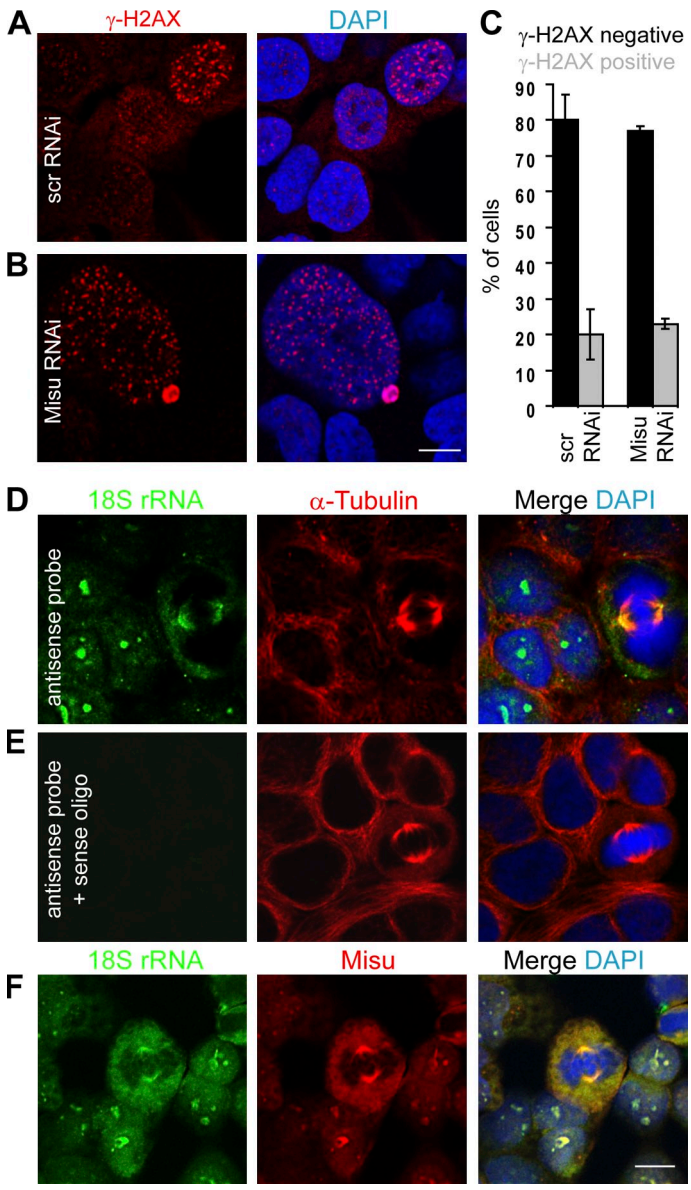

Figure S3. **Depletion of Misu does not result in DNA double-strand breaks and specificity of 18S rRNA probe.** (A and B) Scr and Misu RNAi cells have similar levels of phosphorylated histone γH2A.X (red). DNA is counterstained with DAPI (blue). (C) Quantification of levels of phosphorylated histone γH2A.X. (D and E) Staining of 18S rRNA (green) using an Alexa Fluor 488–labeled DNA probe (D) is lost when incubated with the corresponding sense oligo before staining (E). Spindles are visualized using α-tubulin antibody (red). (F) Colocalization of 18S rRNA (green) and Misu (red) at nucleoli and the spindle. Error bars indicate mean ± SD. Bars, 10 μm.

Published July 13, 2009

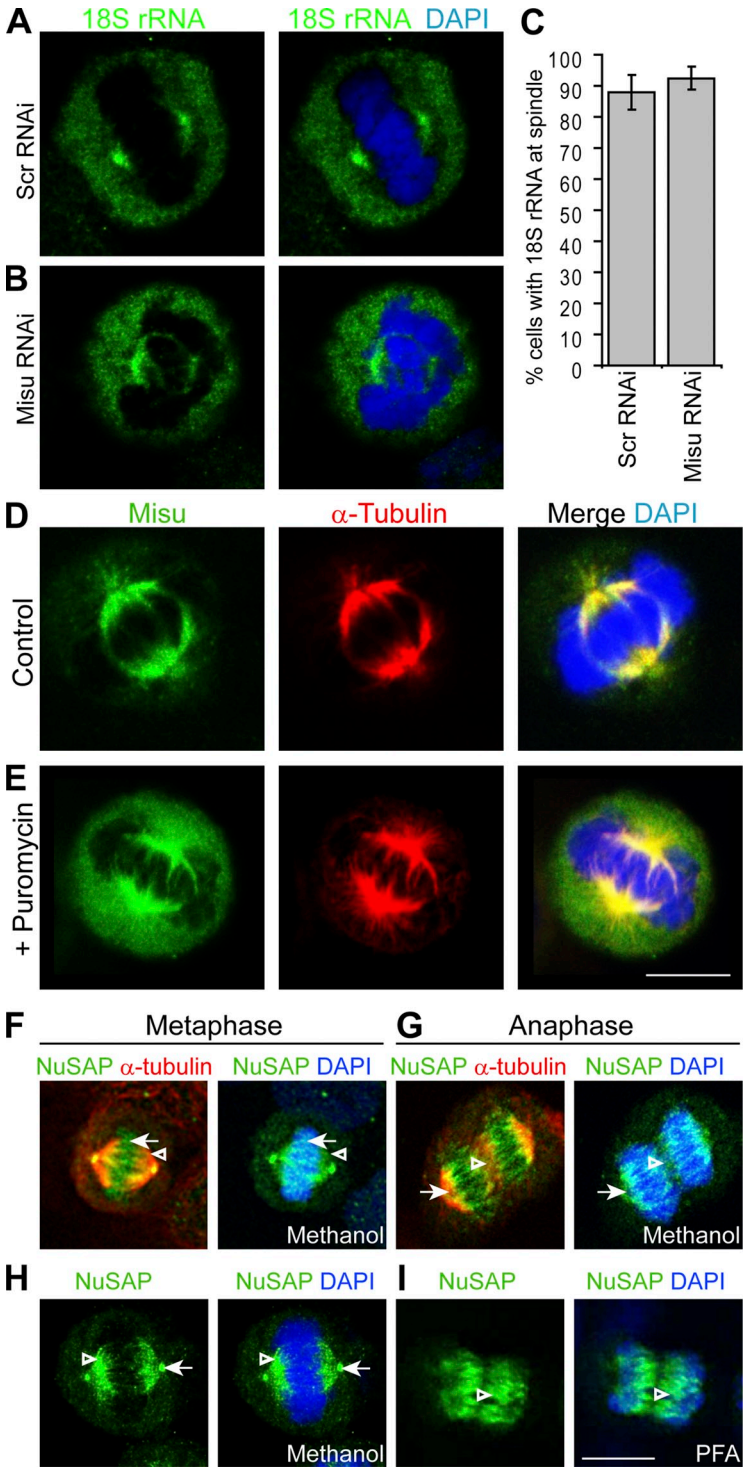

Figure S4. **Localization of 18S rRNA to the spindle is independent of RNA, Misu localizes to the spindle in the absence of active translation, and localization of NuSAP to the spindle varies with cell cycle and fixation method.** (A and B) Localization of 18S rRNA (green) to the spindle is not affected by depletion of Misu using RNAi. DNA is counterstained with DAPI (blue). (C) Quantification for A and B. (D and E) Localization of Misu (green) to the spindle (α-tubulin; D, red) is not affected by treatment with puromycin (E). DNA is counterstained with DAPI. (F–I) NuSAP staining in metaphase (F and H) and anaphase (G and I) varies depending on fixation methods. (F) In some cells, NuSAP labels both the central (arrows) and distal spindle (arrowheads). (G) When fixed with methanol, NuSAP stains both the distal (arrow) and central spindle (arrowhead). (H) In the majority of cells, NuSAP labels the distal spindle with higher intensity (arrowheads) and spindle poles (arrows). (I) When fixed with paraformaldehyde, NuSAP staining can only be found at the central spindle (arrowheads). Error bars indicate mean ± SD. Bars, 10 μm.

Published July 13, 2009

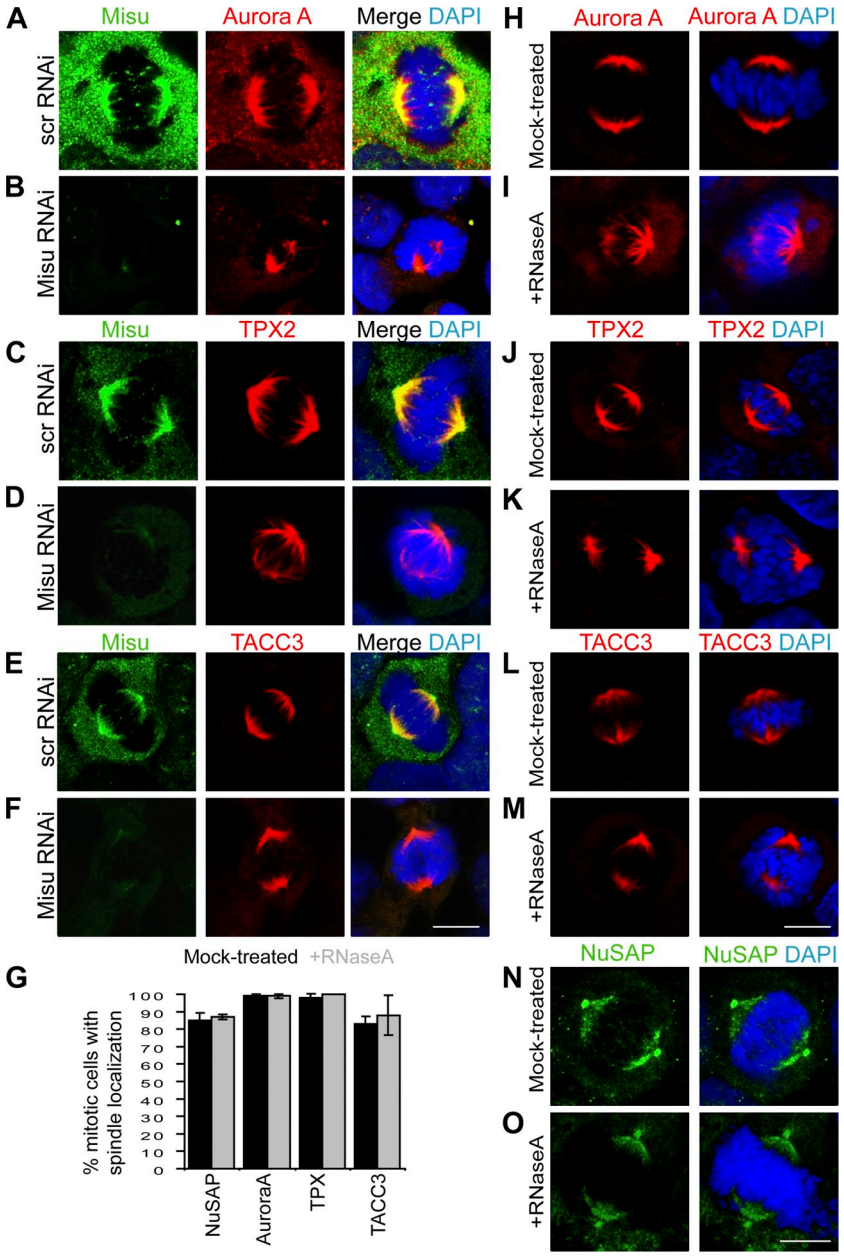

Figure S5. **Depletion of Misu or RNA in HCC1954 cells has no effect on the localization of aurora A, TPX2, or TACC3 during mitosis.** (A–F) Spindle assembly factors aurora A (A and B, red), TPX2 (C and D, red), and TACC3 (E and F, red) localize to the spindle in the presence of Misu (Scr RNAi; A, C, and E, green) and when Misu is depleted by RNAi (Misu RNAi; B, D, and F). (G) Quantification for A–F. (H–P) Spindle assembly factors aurora A (H and I, red), TPX2 (J and K, red), TACC3 (L and M, red), and NuSAP (N and O, green) localize to the spindle when cells are treated with RNase (+RNase; I, K, M, and O). DNA is counterstained with DAPI (blue). Error bars indicate mean ± SD. Bars, 10 µm.